Date of publication xxxx 00, 0000, date of current version xxxx 00, 0000.

Digital Object Identifier 10.1109/ACCESS.2024.0429000

Integrated THz/mmWave Transmission Method for Enhanced URLLC Communications

MOAWIAH ALHULAYIL[1], (Member, IEEE), MOHAMMAD ABU AQOULAH[2], MIGUEL LÓPEZ-BENÍTEZ[3, 4], (Senior Member, IEEE), MAMOUN F. AL-MISTARIHI[2], MOHAMMED ALAMMAR[5], (Member, IEEE), and ABDULRAHMAN AL AYIDH[5]

[1]Department of Electrical Engineering, Applied Science Private University, Amman 11937, Jordan.
[2]Department of Electrical Engineering, Jordan University of Science and Technology, Irbid 22110, Jordan.
[3]Department of Electrical Engineering and Electronics, University of Liverpool, Liverpool, L69 3GJ, United Kingdom.
[4]ARIES Research Centre, Antonio de Nebrija University, 28040 Madrid, Spain.
[5]Department of Electrical Engineering, King Khalid University, Abha 61421, Kingdom of Saudi Arabia.

Corresponding author: Moawiah Alhulayil (e-mail: m_alhulayil@asu.edu.jo).

This work was supported by the Deanship of Research and Graduate Studies at King Khalid University through Small group Research Project under grant number RGP1/251/45.

ABSTRACT Ultra-Reliable and Low-Latency Communication (URLLC) is considered one of the key use cases in the current 5G and future 6G mobile communication networks. In this work, a hybrid transmission scheme is proposed to improve reliability in Terahertz (THz) bands employing adaptive diversity combining at the destination. The proposed scheme combines two links, the first link is a THz link (offering higher capacity but less reliable connectivity) as the main link, and the second link is a millimetre wave (mmWave) link (offering lower capacity but more reliable connectivity) as the backup link. The proposed scheme utilises both links dynamically exploiting the benefits of transmitting over both frequency bands by changing between the main link only and joint main/backup links based on the instantaneous quality of the channel for the main link. The received signals are combined at the destination using Selection Combining (SC) and Maximal Ratio Combining (MRC). The performance of the proposed scheme is evaluated analytically considering the Fluctuating Two-Ray (FTR) and $\alpha - \mu$ models for the mmWave and THz links, respectively. The obtained results show that the proposed hybrid transmission scheme achieves the same reliability provided by the continuous dual-link transmission scheme, where both links (THz and mmWave links) are used continuously for transmission, thus making the proposed scheme an appropriate solution to provide URLLC applications in a resource-efficient manner.

INDEX TERMS 5G new radio, 6G, Terahertz communication, millimetre wave communication, ultra-reliable low-latency communication.

I. INTRODUCTION

Ultra-Reliable and Low-Latency Communication (URLLC) in current 5G and future 6G mobile communication networks is a crucial obstacle due to the strict constraints on reliability and latency. This type of communication scenario is created to offer highly dependable, low latency and time-sensitive communication services in support of a variety of applications such as autonomous driving, industrial automation and healthcare [1], [2].

Although 5G technology significantly outperforms earlier wireless technology generations, there is still a demand for even more reliable and fast communication solutions. Therefore, millimetre wave (mmWave) communication, which uses the extremely high frequency range from 30 to 300 GHz [3], is presented as a key solution that can offer substantially faster data transmission rates and reduced latency compared to earlier generations because of its capacity to operate at extremely high frequencies [4], [5]. mmWave is an innovative 5G technology that plays a key role in meeting the ever-increasing demand of data-intensive applications such as video streaming, virtual reality, real-time gaming and the Internet of Things (IoTs) [6], [7]. Moreover, small-cell wireless networks can be deployed using this technology due to the short wavelengths of mmWave signals providing high connectivity in densely populated places [8].

Based on the success of mmWave communication, there was a logical sense to explore higher radio frequency bands, primarily the Terahertz (THz) band. The THz band is defined

as the frequency range from 0.1 to 10 THz [9], [10]. THz frequencies are anticipated to be essential in the development of the upcoming 6G technology due to their capacity to offer extraordinarily fast data transmission speeds and minimal latency. Using THz technology is appropriate for several applications such as virtual and augmented reality, medical imaging and autonomous vehicles [11]. THz bands attracted researchers due to its ability to fulfil the continuously growing demand for data speeds as we move into imminent beyond 5G systems and projected 6G systems. In particular, due to its potential to offer a significant amount of bandwidth, the THz band is thought to be one of the major enablers for wireless communications beyond 5G, supporting a significant number of connected devices and extremely high user data rates [12]. For instance, it is already widely acknowledged that THz communications will play a crucial role in the next 6G systems [13]. Although there are many obstacles such as wireless channel modelling, signal processing and system security, there is a growing body of research devoted to creating THz communication technology because of the significant potential advantages of THz bands for 6G networks [14]. In particular, a greater bandwidth is offered by the THz band compared to the mmWave band providing higher data rates and lower interference [15]. In addition, higher link directionality is allowed in the THz band compared to the mmWave band owing to shorter wavelengths and lower free-space diffraction. Moreover, due to high directionality of THz beams, lower risk of eavesdropping is presented in the THz band compared to the mmWave band. The upcoming generations of wireless communication are expected to heavily rely on THz communication [16]–[18].

However, propagation in THz bands is challenging, which makes the provision of URLLC services problematic. Multi-Connectivity (MC) has been proposed as a reliability enhancement feature to satisfy the demanding key performance indicators for URLLC. This can be achieved by establishing several parallel connections between the transmitter and receiver improving data reliability through path redundancy for URLLC. This duplication of data significantly improves the probability of the data reception at the expense of resource usage [19]–[21]. Several methods and techniques have been proposed in the literature to achieve the challenging reliability requirement of URLLC using MC schemes at different levels of complexity. The proposed works can achieve the reliability requirement of URLLC at the expense of lower system capacity [22]. Hybrid transmission techniques are considered a hot topic that have recently attracted remarkable research interests [23]. In this communication scheme, the signal is transmitted over multiple frequency bands using adaptive combining techniques at the destination. This helps in achieving redundancy and leads to a better performance. Several works have been conducted to study the statistical characteristics of hybrid links over different frequency bands; however, most existing works have explored this idea only in the context of Free-Space Optical (FSO) communication [24]–[27], while its application to other relevant wireless communication scenarios as the one considered in this work has received very limited attention. In particular, [25] analyses dual-hop Radio-Frequency/Free-Space Optical (RF/FSO) relaying systems with imperfect Channel State Information (CSI). The study derives outage probability, bit-error rate and effective capacity expressions for both Amplify-and-Forward (AF) and Decode-and-Forward (DF) relaying. The obtained results show that Maximal Ratio Combining (MRC)-based relaying enhances Signal-to-Noise Ratio (SNR) performance, but imperfect CSI introduces an error floor, affecting system reliability. [26] introduces a hybrid FSO/THz-based backhaul network designed to provide high data rate and reliable communication for terrestrial mobile users operating at mmWave frequencies. The study accounts for the challenges posed by atmospheric turbulence, pointing errors in FSO links and the high path loss of THz channels. A soft-switching method is proposed to reduce the frequent back-and-forth switching between links improving network stability. The obtained results demonstrate that the joint implementation of FSO and THz links enhances system reliability and data rates while minimizing switching overhead. [27] proposes a hybrid FSO/RF communication system with adaptive link selection, where the RF link is activated only when the FSO link's quality degrades. The study derives outage probability expressions and demonstrates that MRC combining improves system reliability under atmospheric turbulence. The obtained results confirm that the proposed scheme with adaptive combining outperforms standalone FSO and RF systems in terms of outage performance across different weather conditions and turbulence regimes. [28] analyses a hybrid THz/mmWave network using a Poisson Cluster Process (PCP) model, where THz nodes cluster around mmWave nodes. The study derives interference expressions and evaluates coverage probability, showing that optimal clustering enhances network performance and mitigates blockage effects. The proposed framework outperforms traditional Poisson Point Process (PPP)-based networks, offering a practical approach for extending THz communication coverage.

However, despite extensive research on THz and mmWave communications, existing approaches have notable limitations. Previous studies primarily focus on either THz or mmWave transmission individually, failing to address the combined reliability and latency challenges inherent in these high-frequency bands [14], [29]–[31]. Single-band transmission methods struggle with severe path loss, atmospheric attenuation and blockages making them unsuitable for URLLC applications that require continuous and ultra-reliable connectivity. On the other hand, previous dual-link architectures often operate both links simultaneously leading to inefficient resource allocation and increased power consumption. In addition, previous research lacks an adaptive hybrid mechanism that dynamically switches between THz and mmWave links based on real-time channel conditions. In contrast, our proposed method implements an adaptive hybrid transmission mechanism that dynamically switches between THz and mmWave links based on real-time channel conditions ensur-

TABLE 1. Comparative analysis of hybrid communication systems.

Work	Frequency Band	Diversity Technique	Key Characteristics	Limitations
[25]	RF/FSO	Dual-Hop Relaying with Imperfect CSI	Derives outage probability and effective capacity expressions; demonstrating MRC-based relaying improves SNR performance.	Performance degradation due to CSI estimation errors.
[26]	FSO/THz	Soft-switching mechanism	Proposes hybrid FSO/THz backhaul network for high-data-rate terrestrial users; mitigates frequent switching.	Limited analysis on real-time adaptive switching performance.
[27]	FSO/RF	Adaptive link selection with MRC	Utilises adaptive link selection; activating RF only when FSO quality degrades; improving reliability in adverse conditions.	Requires hard switching; performance affected by atmospheric conditions.
[28]	THz/mmWave	Spatial diversity via Poisson Cluster Process (PCP)	Evaluates interference in hybrid THz/mmWave networks; showing optimal clustering improves coverage probability.	Requires high computational complexity for real-time clustering adjustments.
Proposed scheme	THz/mmWave	Adaptive link selection with SC & MRC	Dynamically switches between THz and mmWave based on real-time SNR; enhances reliability and efficiency.	Requires real-time channel estimation.

ing both high capacity and reliability. In addition, we incorporate Selection Combining (SC) and Maximal Ratio Combining (MRC) at the destination to optimise signal reception balancing performance trade-offs efficiently. Furthermore, we perform an analytical evaluation using realistic fading models, namely the Fluctuating Two-Ray (FTR) and $\alpha - \mu$ models for the mmWave and THz channels, respectively, to accurately characterise system reliability under practical network conditions. By integrating adaptive switching, advanced diversity techniques and rigorous channel modelling, our approach enhances URLLC performance, optimises spectral efficiency and reduces unnecessary energy consumption compared to previous works. A structured comparison highlighting the key differences and limitations between prior works and the proposed approach is provided in Table 1.

This work focuses on solving the challenge of maintaining both ultra-reliability and low latency in high-frequency bands. Traditional single-band communication approaches struggle to achieve the strict requirements of URLLC due to the severe path loss and environmental unreliability of THz and mmWave signals. Our proposed solution integrates both frequency bands to dynamically adapt transmission, ensuring a continuous and stable link even in fluctuating channel conditions. This method enhances the reliability of URLLC systems making it a promising approach for future wireless networks. In particular, a novel Physical (PHY) layer MC technique is proposed in this work to benefit from the complementary properties of THz and mmWave frequency bands. In particular, the larger bandwidths available in the THz spectrum and its rather minimal use make the THz band a favoured option for the supply of high data rates. However, in terms of propagation attenuation, THz waves experience higher path loss and signal blockage than mmWaves. This would lead to unstable connectivity and unreliable communication while propagating over THz bands [14], [32]. To leverage the complementary characteristics of both frequency bands (i.e., higher reliability of mmWave bands and higher capacity of THz bands) effectively, a novel scheme is proposed in this work for hybrid THz/mmWave transmission with adaptive combining at the destination. The choice of THz and mmWave bands in the proposed scheme is motivated by their complementary characteristics. THz enables ultra-high-speed transmission but suffers from severe path loss and limited coverage, whereas mmWave provides a more reliable backup link while maintaining high data rates. Other frequency bands, such as Sub-6 GHz, were not considered in this study due to their significantly lower data rates, which would not meet the URLLC requirements. This selection aligns with emerging 5G and 6G communication frameworks, where both THz and mmWave bands are envisioned as key enablers of next-generation wireless networks. A THz link is used as the main communication link providing high capacity, while a mmWave link is used as a backup link to enhance reliability when required. The THz link is used alone for transmission provided that the instantaneous SNR is greater than a certain threshold guaranteeing an acceptable quality. Under this scenario, the mmWave link either stays in standby mode or is utilised for other data transmissions. When the main link (THz link) quality degrades (i.e., its instantaneous SNR goes below a certain threshold) then the backup link (mmWave link) is activated in parallel to the main link in order to increase reliability. Both THz/mmWave links are then combined with a diversity technique at the destination. When the THz link quality recovers, the transmission goes back only over the THz link, leaving the mmWave link in standby mode or releasing it for other data transmissions. The proposed hybrid scheme allows to gain concurrently from the reliability of mmWave bands and the capacity of THz bands. In addition, compared to the dual-transmission approach where

both THz and mmWave links operate simultaneously [33], the proposed scheme conserves energy and minimises interference by keeping the backup mmWave link in standby mode. Moreover, it enhances radio resource efficiency when the mmWave link is utilised for alternate data transmissions. This adaptive hybrid scheme inherently accounts for environmental variations including user mobility, interference and atmospheric conditions by dynamically switching between THz and mmWave links based on real-time channel assessment. This ensures reliable and uninterrupted communication even in challenging network scenarios.

This work follows a link-level approach, focusing on SNR as the main performance metric. While a system-level analysis incorporating interference effects (Signal-to-Interference Ratio (SIR)) could be explored in future studies, it does not impact the fundamental advantages of the proposed hybrid scheme. Moreover, advanced techniques such as beamforming and Intelligent Reflecting Surfaces (IRS) help mitigate interference by directing signals toward the intended receiver reducing its impact. On the other hand, blockage modelling is an important aspect of THz and mmWave communication systems, as it primarily affects the path loss component of radio propagation. According to 3GPP Line-of-Sight (LoS) and Non-Line-of-Sight (NLoS) probabilistic models, blockage leads to a reduction in the average SNR rather than complete communication failure. The fading models used in this work focus on the multi-path component and can be adjusted to account for blockage effects by incorporating a lower average SNR and adjusting the fading parameters accordingly. Therefore, the proposed hybrid THz/mmWave transmission scheme remains functional, with necessary adjustments to reflect real-world operating conditions.

The contributions of this work are summarised below:

- The SNR statistics at the destination of the proposed hybrid transmission scheme are derived. The analysis is carried out employing Selection Combining (SC) and Maximal Ratio Combining (MRC) techniques.
- The probability of outage and the probability of using the backup mmWave link under both diversity techniques are provided in terms of the communication distance. Moreover, the optimum switching threshold for the THz/mmWave hybrid transmission scheme achieving the highest communication reliability is also addressed.
- Analytical expressions are derived for the bit-error performance of the proposed hybrid scheme under several configurations using SC and MRC techniques, which are employed to demonstrate the benefits of the proposed transmission scheme in terms of reliability.

The remainder of this work is organised as follows. First, Section II describes the system model considered in this work. In addition, the proposed hybrid transmission scheme is introduced. Analytical expressions for the SNR statistics are derived at the destination under SC and MRC techniques in Section III. Further analytical expressions for the outage probability, backup link usage probability and bit-error rate

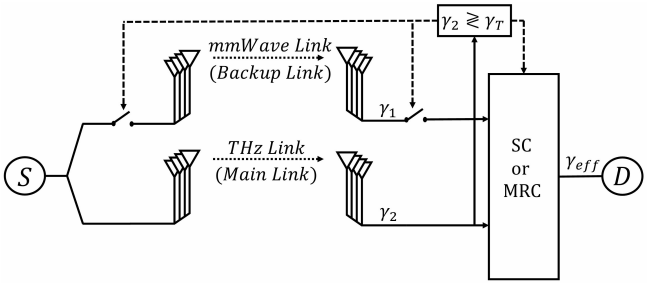

FIGURE 1. Hybrid THz/mmWave transmission scheme.

of the proposed hybrid transmission scheme are derived in Section IV. The evaluation scenario is presented along with the evaluation for the performance of the proposed hybrid transmission scheme in Section V. The conclusions are summarised in Section VI. Finally, potential research directions for future work are discussed in Section VII.

II. SYSTEM MODEL

The proposed hybrid transmission system is illustrated in Fig. 1. Specifically, two links are considered between the source (S) and destination (D) in this hybrid system; the THz link, which is the primary communication link, and the mmWave link, which is the secondary link that is used as a backup link for the THz link. The main link (THz link) is always active while the backup link (mmWave link) remains in standby mode until the instantaneous SNR of the main link, γ_2, becomes lower than a certain threshold γ_T. This threshold, γ_T, is the minimum SNR required to deliver the desired link performance in terms of the Bit Error Rate (BER). When γ_2 becomes lower than γ_T, the activation for the backup link is achieved by a feedback signal from the destination to the source and then the source transmits the same data over the two links. On the other hand, when γ_2 becomes higher than γ_T, a feedback signal is sent to the source by the destination to deactivate the backup link and thus the communication proceeds via the main link only.

In this context, SC and MRC diversity techniques are employed at the destination to combine the received signals from both links when they are in operation simultaneously. SC selects the strongest signal based on the highest instantaneous SNR, which is given by $\max(\gamma_1, \gamma_2)$ [34, eq. (6.6)]. On the other hand, MRC averages the signals from both links, weighted by their respective channel impulse responses. MRC maximises the effective SNR at the combiner output and is higher than the instantaneous SNR of each link individually, which is given by $\gamma_1 + \gamma_2$ [34, eq. (6.22)]. MRC has a higher gain and is more robust against noise compared to SC, however it is more complex due to the required signal processing and channel estimation [34].

For the mmWave link fading, the Fluctuating Two-Ray (FTR) model is considered [35]. Based on this model, the Probability Density Function (PDF) and Cumulative Distribution Function (CDF) of the instantaneous SNR per symbol,

γ_1, are expressed, respectively, as [36, eq. (6)–(8)]

$$f_{\gamma_1}(x) = \frac{m^m}{\Gamma(m)} \sum_{j=0}^{\infty} \frac{K^j d_j}{(j!)^2} \frac{x^j}{(2\sigma^2)^{j+1}} \exp\left(-\frac{x}{2\sigma^2}\right) \quad (1)$$

$$F_{\gamma_1}(x) = \frac{m^m}{\Gamma(m)} \sum_{j=0}^{\infty} \frac{K^j d_j}{(j!)^2} \gamma\left(j+1, \frac{x}{2\sigma^2}\right) \quad (2)$$

where m is the fading severity index, K is the ratio between the average powers in the specular/dominant and the diffuse/scattered multipath components, $2\sigma^2$ is the total power of the diffuse components, $\Gamma(\cdot)$ is the standard gamma function [37, eq. (8.310.1)], $\gamma(\cdot,\cdot)$ is the lower incomplete gamma function [37, eq. (8.350.1)], and d_j is [38, eq. (13)]

$$d_j \triangleq \sum_{k=0}^{j} \binom{j}{k} \left(\frac{\Delta}{2}\right)^k \sum_{l=0}^{k} \binom{k}{l} \frac{\Gamma(j+m+2l-k)}{\left((m+K)^2-(K\Delta)^2\right)^{\frac{j+m}{2}}} \times (-1)^{2l-k} P_{j+m-1}^{k-2l}\left(\frac{m+K}{\sqrt{(m+K)^2-(K\Delta)^2}}\right) \quad (3)$$

where the parameter $\Delta \in [0,1]$ characterises the similarity of the two dominant waves (for $\Delta = 0$ one of them is zero and for $\Delta = 1$ both are equal) and $P_\nu^\mu(\cdot)$ is the associated Legendre function (or spherical function) of the first kind [37, eq. (8.702)]. An alternative expression for d_j is given by [38, eq. (19)]. In the FTR model, the average SNR is obtained as $\overline{\gamma}_1 = (E_b/N_0)2\sigma^2(1+K)$, where E_b/N_0 is the energy per bit to noise power spectral density ratio.

For the THz link fading, the instantaneous SNR per symbol, γ_2, follows $\alpha-\mu$ distribution [39], [40]. Its PDF and CDF are given, respectively, by [41, eqs. (3) and (4)]

$$f_{\gamma_2}(x) = \frac{\alpha\mu^\mu \left(\frac{x}{\overline{\gamma}_2}\right)^{\alpha\mu/2-1} \exp\left(-\mu\left(\frac{x}{\overline{\gamma}_2}\right)^{\alpha/2}\right)}{2\overline{\gamma}_2\Gamma(\mu)} \quad (4)$$

$$F_{\gamma_2}(x) = \frac{\gamma\left(\mu, \mu\left(\frac{x}{\overline{\gamma}_2}\right)^{\alpha/2}\right)}{\Gamma(\mu)} \quad (5)$$

The upper incomplete gamma function can be used to express (5) as follows [37, eq. (8.356.3)]

$$F_{\gamma_2}(x) = 1 - \frac{\Gamma\left(\mu, \mu\left(\frac{x}{\overline{\gamma}_2}\right)^{\alpha/2}\right)}{\Gamma(\mu)} \quad (6)$$

where $\alpha > 0$ represents the non-linearity on the received signal envelope, $\mu > 0$ represents the number of multipath components of the received signal, $\Gamma(\cdot)$ is the gamma function [37, eq. (8.310.1)], and $\Gamma(a,x) = \int_x^\infty t^{a-1}e^{-t}dt$ represents the upper incomplete gamma function [37, eq. (8.350.2)]. Notably, the FTR model is widely accepted as an accurate representation of mmWave fading channels, as it effectively captures multipath fading characteristics with a dominant LoS component. Similarly, the $\alpha-\mu$ model is recognised as a general fading model suitable for THz communications, providing flexibility in modelling different propagation conditions. These models have been extensively validated in the literature and are well-suited for characterising small-scale fading effects in their respective frequency bands.

It is worth mentioning that the proposed scheme effectively adapts to varying network conditions, including high user density and rapid channel fluctuations. The adaptive link selection ensures seamless transitions between THz and mmWave links mitigating congestion while maintaining connectivity. In addition, diversity combining enhances signal reception and minimises outage probability reinforcing the system's robustness in dynamic URLLC environments. However, the computational complexity of the proposed scheme is primarily influenced by adaptive link selection and diversity combing techniques. The link selection process involves real-time channel quality assessment activating the mmWave link only when the THz link's SNR drops below a predefined threshold. As this relies on simple threshold comparisons, the computational overhead remains minimal. For diversity combining, SC selects the strongest signal with minimal processing, whereas MRC applies weighted signal processing, requiring additional computations. However, both techniques remain computationally feasible for real-time URLLC applications. The proposed scheme ensures a balance between reliability and computational efficiency making it practical for deployment.

From a practical deployment perspective, the proposed hybrid scheme is well-suited for integration into future 5G and 6G networks, leveraging advancements in high-frequency spectrum utilisation and intelligent radio resource management. However, key challenges must be addressed including beam alignment accuracy, channel estimation complexity and network densification requirements. The sensitivity of THz signals to blockages and environmental factors necessitates robust beam tracking and adaptive reconfiguration mechanisms. On the other hand, from an energy efficiency perspective, the proposed scheme leverages adaptive link selection to minimise unnecessary transmissions over the mmWave link, significantly reducing power consumption while maintaining reliability. Unlike continuous dual-link transmission, where the mmWave link remains active at all times, our approach dynamically activates the backup link only when needed, leading to substantial energy savings. In addition, the scheme maintains low computational complexity, as link selection involves simple threshold-based comparisons, which are already performed in modern wireless systems. The SC technique ensures minimal processing overhead by selecting the strongest signal, while MRC applies weighted signal processing for optimal reception, adding only a marginal computational burden. As both techniques rely on lightweight mathematical operations, the scheme is computationally efficient and well-suited for real-time URLLC deployment with minimal energy overhead.

The proposed hybrid THz/mmWave transmission scheme requires minimal hardware modifications as Beyond 5G (B5G) and 6G networks are expected to support both mmWave and THz bands, with many commercial 5G devices already operating in mmWave frequencies. Signal quality

estimation for link adaptation aligns with 3GPP standards, ensuring seamless integration. In addition, the scheme leverages widely used diversity combining techniques (SC/MRC), which are already supported in existing infrastructure, making implementation cost-effective and practical.

III. ANALYSIS OF SNR STATISTICS

A. DISTRIBUTION OF THE SNR USING SC

As shown in Fig. 1, the instantaneous effective SNR at the destination, denoted by γ_{eff}, depends on the predefined threshold γ_T. In particular, when $\gamma_2 > \gamma_T$, the main link only is in operation and thus $\gamma_{\text{eff}} = \gamma_2$. On the other hand, when $\gamma_2 \leq \gamma_T$, the backup link is activated and γ_{eff} depends on the considered diversity technique. Therefore, the CDF of the instantaneous effective SNR can be written as

$$F_{\gamma_{\text{eff}}}(x) = P\big(g(\gamma_1,\gamma_2) \leq x, \gamma_2 \leq \gamma_T\big) + P\big(\gamma_2 \leq x, \gamma_2 > \gamma_T\big) \tag{7}$$

where $g(\gamma_1,\gamma_2)$ represents the effective SNR at the output of the selected diversity technique in terms of the SNR for each individual link. Hence, $g(\gamma_1,\gamma_2) = \max(\gamma_1,\gamma_2)$ for SC [34, eq. (6.6)] and thus (7) can be customised for SC as follows

$$F_{\gamma_{\text{eff}}}(x) = P\big(\max(\gamma_1,\gamma_2) \leq x, \gamma_2 \leq \gamma_T\big) + P\big(\gamma_2 \leq x, \gamma_2 > \gamma_T\big) \tag{8}$$

Theorem 1 (CDF of SNR under SC)**.** *The CDF of SNR for the proposed hybrid system under SC is given by (9).*

Proof. (8) can be expressed in terms of the associated conditional probabilities as

$$F_{\gamma_{\text{eff}}}(x) = P(\max(\gamma_1,\gamma_2) \leq x \,|\, \gamma_2 \leq \gamma_T) P(\gamma_2 \leq \gamma_T) \tag{10}$$
$$+ P(\gamma_2 \leq x \,|\, \gamma_2 > \gamma_T) P(\gamma_2 > \gamma_T) \tag{11}$$

The conditional probability in (10) can be expressed as

$$P(\max(\gamma_1,\gamma_2) \leq x \,|\, \gamma_2 \leq \gamma_T) = P(\gamma_1 \leq x) P(\gamma_2 \leq x \mid \gamma_2 \leq \gamma_T) = F_{\gamma_1}(x) \cdot \min\left(1, \frac{F_{\gamma_2}(x)}{F_{\gamma_2}(\gamma_T)}\right) \tag{12}$$

The conditional probability in (11) can be expressed as

$$P\left(\gamma_2 \leq x \mid \gamma_2 > \gamma_T\right) = \mathbf{1}_{(\gamma_T,\infty)}(x) \cdot \frac{F_{\gamma_2}(x) - F_{\gamma_2}(\gamma_T)}{1 - F_{\gamma_2}(\gamma_T)} \tag{13}$$

where $\mathbf{1}_A(x)$ is the indicator function of A, which is equal to one when $x \in A$ and zero otherwise. Hence, introducing (12) and (13) in (10) and (11), respectively, and simplifying yields

$$F_{\gamma_{\text{eff}}}(x) = F_{\gamma_1}(x) \cdot \min\left(F_{\gamma_2}(x), F_{\gamma_2}(\gamma_T)\right) + \mathbf{1}_{(\gamma_T,\infty)}(x) \cdot \left[F_{\gamma_2}(x) - F_{\gamma_2}(\gamma_T)\right] \tag{14}$$

However, the expression in (14) can be rewritten as follows [23, eq. (14)]

$$F_{\gamma_{\text{eff}}}(x) = \begin{cases} F_{\gamma_1}(x) F_{\gamma_2}(x), & x \leq \gamma_T \quad (15a) \\ F_{\gamma_1}(x) F_{\gamma_2}(\gamma_T) + F_{\gamma_2}(x) - F_{\gamma_2}(\gamma_T), & x > \gamma_T \quad (15b) \end{cases}$$

Introducing (2) and (6) in (15a) yields (9a). Similarly, introducing (2) and (6) in (15b) and simplifying yields (9b). □

Theorem 2 (PDF of SNR under SC)**.** *The PDF of SNR for the proposed hybrid system under SC is given by (16).*

Proof. When $\gamma_2 \leq \gamma_T$, the differentiation of (9a) using [37, eq. (8.356.4)] yields

$$\begin{aligned} f_{\gamma_{\text{eff}}}(x) &= \frac{m^m}{\Gamma(m)} \sum_{j=0}^{\infty} \frac{K^j d_j}{(j!)^2} \frac{x^j}{(2\sigma^2)^{j+1}} \exp\left(-\frac{x}{2\sigma^2}\right) \\ &\times \left[1 - \frac{\Gamma\left(\mu, \mu\left(\frac{x}{\bar{\gamma}_2}\right)^{\alpha/2}\right)}{\Gamma(\mu)}\right] \\ &+ \frac{m^m}{\Gamma(m)} \sum_{j=0}^{\infty} \frac{K^j d_j}{(j!)^2} \gamma\left(j+1, \frac{x}{2\sigma^2}\right) \\ &\times \frac{\alpha\mu^\mu \left(\frac{x}{\bar{\gamma}_2}\right)^{\alpha\mu/2-1} \exp\left(-\mu\left(\frac{x}{\bar{\gamma}_2}\right)^{\alpha/2}\right)}{2\bar{\gamma}_2 \Gamma(\mu)} \end{aligned} \tag{17}$$

Employing the commutative and associative properties of summation yields (16a). Similarly, when $\gamma_2 > \gamma_T$, the differentiation of (9b) yields (16b). □

B. DISTRIBUTION OF THE SNR USING MRC

Theorem 3 (PDF of SNR under MRC)**.** *The PDF of SNR for the proposed hybrid system under MRC is given by (18).*

Proof. When $\gamma_2 \leq \gamma_T$, the PDF of the instantaneous effective SNR under MRC can be written as follows [42, eq. (6-45)]

$$f_{\gamma_{\text{eff}}}(x) = \int_0^x f_{\gamma_1}(x-y) f_{\gamma_2}(y) dy \tag{19}$$

$$= \frac{\alpha\mu^\mu m^m}{2\bar{\gamma}_2^{\alpha\mu/2}\Gamma(\mu)\Gamma(m)} \sum_{j=0}^{\infty} \frac{K^j d_j}{(j!)^2} \frac{1}{(2\sigma^2)^{j+1}} \exp\left(-\frac{x}{2\sigma^2}\right) \times \int_0^x (x-y)^j y^{\alpha\mu/2-1} \exp\left(\frac{y}{2\sigma^2} - \mu\left(\frac{y}{\bar{\gamma}_2}\right)^{\alpha/2}\right) dy, \; x \leq \gamma_T \tag{20}$$

Using the series expansion [37, eq. (1.111)] and simplifying the result, (20) can be written as

$$f_{\gamma_{\text{eff}}}(x) = \frac{\alpha\mu^\mu m^m}{2\bar{\gamma}_2^{\alpha\mu/2}\Gamma(\mu)\Gamma(m)} \sum_{j=0}^{\infty} \sum_{i=0}^{j} \binom{j}{i} \frac{K^j d_j}{(j!)^2} \frac{1}{(2\sigma^2)^{j+1}} \exp\left(-\frac{x}{2\sigma^2}\right) \times (-1)^i x^{j-i} \int_0^x y^{\alpha\mu/2+i-1} \exp\left(\frac{y}{2\sigma^2} - \mu\left(\frac{y}{\bar{\gamma}_2}\right)^{\alpha/2}\right) dy, \; x \leq \gamma_T \tag{21}$$

To the best of the authors' knowledge, there is no reported elementary solution for the integral in (21). However, (21) can be simplified using the infinite series representation of the exponential function as follows [37, eq. (1.211)]

$$f_{\gamma_{\text{eff}}}(x) = \frac{\alpha\mu^\mu m^m}{2\bar{\gamma}_2^{\alpha\mu/2}\Gamma(\mu)\Gamma(m)} \sum_{j=0}^{\infty} \sum_{n=0}^{\infty} \sum_{i=0}^{j} \binom{j}{i} \frac{K^j d_j}{(j!)^2} \frac{1}{(2\sigma^2)^{j+n+1}} \exp\left(-\frac{x}{2\sigma^2}\right) \times \frac{(-1)^i x^{j-i}}{n!} \int_0^x y^{\alpha\mu/2+i+n-1} \exp\left(-\mu\left(\frac{y}{\bar{\gamma}_2}\right)^{\alpha/2}\right) dy, \; x \leq \gamma_T \tag{22}$$

The solution to the integral in (22) can be obtained with the aid of [37, eq. (3.381.8)], which yields

$$\int_0^x y^{\alpha\mu/2+i+n-1}\exp\left(-\mu\left(\frac{y}{\bar{\gamma}_2}\right)^{\alpha/2}\right)dy=\frac{2\bar{\gamma}_2^{\alpha v/2}}{\alpha\mu^v}\gamma\left(v,\mu\left(\frac{x}{\bar{\gamma}_2}\right)^{\alpha/2}\right) \tag{23}$$

where $v=\frac{\alpha\mu+2i+2n}{\alpha}$.
Introducing (23) in (22) and grouping terms yields (18a). On the other hand, when $\gamma_2>\gamma_T$, the PDF of the instantaneous effective SNR under MRC can be obtained by differentiating (24b), derived as shown below, which completes the proof. □

Theorem 4 (CDF of SNR under MRC)**.** *The CDF of SNR for the proposed hybrid system under MRC is given by (24).*

Proof. When $\gamma_2\le\gamma_T$, (24a) can be obtained by integrating the PDF in (18a) as follows

$$F_{\gamma_{\text{eff}}}(x)=\int_0^x f_{\gamma_{\text{eff}}}(y)dy \tag{26}$$

$$=\frac{\mu^\mu m^m}{\Gamma(\mu)\Gamma(m)}\sum_{j=0}^{\infty}\sum_{n=0}^{\infty}\sum_{i=0}^{j}\binom{j}{i}\frac{K^j d_j}{(j!)^2}\frac{(-1)^i}{(2\sigma^2)^{n+j+1}n!}\frac{\bar{\gamma}_2^{\alpha(v-\mu)/2}}{\mu^v}\times\int_0^x y^{j-i}\exp\left(-\frac{y}{2\sigma^2}\right)\gamma\left(v,\mu\left(\frac{y}{\bar{\gamma}_2}\right)^{\alpha/2}\right)dy,\ x\le\gamma_T \tag{27}$$

$$F_{\gamma_{\text{eff}}}(x)=\begin{cases}\left[1-\dfrac{\Gamma\left(\mu,\mu\left(\frac{x}{\bar{\gamma}_2}\right)^{\alpha/2}\right)}{\Gamma(\mu)}\right]\times\dfrac{m^m}{\Gamma(m)}\displaystyle\sum_{j=0}^{\infty}\frac{K^j d_j}{(j!)^2}\,\gamma\left(j+1,\frac{x}{2\sigma^2}\right), & x\le\gamma_T \quad (9a)\\ \left[1-\dfrac{\Gamma\left(\mu,\mu\left(\frac{x}{\bar{\gamma}_2}\right)^{\alpha/2}\right)}{\Gamma(\mu)}\right]+\left[1-\dfrac{\Gamma\left(\mu,\mu\left(\frac{\gamma_T}{\bar{\gamma}_2}\right)^{\alpha/2}\right)}{\Gamma(\mu)}\right]\times\left[\dfrac{m^m}{\Gamma(m)}\displaystyle\sum_{j=0}^{\infty}\frac{K^j d_j}{(j!)^2}\,\gamma\left(j+1,\frac{x}{2\sigma^2}\right)-1\right], & x>\gamma_T \quad (9b)\end{cases}$$

$$f_{\gamma_{\text{eff}}}(x)=\begin{cases}\dfrac{m^m}{\Gamma(m)}\displaystyle\sum_{j=0}^{\infty}\frac{K^j d_j}{(j!)^2}\left\{\frac{x^j}{(2\sigma^2)^{j+1}}\exp\left(-\frac{x}{2\sigma^2}\right)\left[1-\frac{\Gamma\left(\mu,\mu\left(\frac{x}{\bar{\gamma}_2}\right)^{\alpha/2}\right)}{\Gamma(\mu)}\right]+\gamma(j+1,\frac{x}{2\sigma^2})\frac{\alpha\mu^\mu\left(\frac{x}{\bar{\gamma}_2}\right)^{\alpha\mu/2-1}\exp\left(-\mu\left(\frac{x}{\bar{\gamma}_2}\right)^{\alpha/2}\right)}{2\bar{\gamma}_2\Gamma(\mu)}\right\}, & x\le\gamma_T \quad (16a)\\ \dfrac{\alpha\mu^\mu\left(\frac{x}{\bar{\gamma}_2}\right)^{\alpha\mu/2-1}\exp\left(-\mu\left(\frac{x}{\bar{\gamma}_2}\right)^{\alpha/2}\right)}{2\bar{\gamma}_2\Gamma(\mu)}+\left[1-\dfrac{\Gamma\left(\mu,\mu\left(\frac{\gamma_T}{\bar{\gamma}_2}\right)^{\alpha/2}\right)}{\Gamma(\mu)}\right]\times\dfrac{m^m}{\Gamma(m)}\displaystyle\sum_{j=0}^{\infty}\frac{K^j d_j}{(j!)^2}\frac{x^j}{(2\sigma^2)^{j+1}}\exp\left(-\frac{x}{2\sigma^2}\right), & x>\gamma_T \quad (16b)\end{cases}$$

$$f_{\gamma_{\text{eff}}}(x)=\begin{cases}\dfrac{\mu^\mu m^m}{\Gamma(\mu)\Gamma(m)}\displaystyle\sum_{j=0}^{\infty}\sum_{n=0}^{\infty}\sum_{i=0}^{j}\binom{j}{i}\frac{K^j d_j}{(j!)^2}\exp\left(-\frac{x}{2\sigma^2}\right)\times\frac{(-1)^i x^{j-i}}{(2\sigma^2)^{n+j+1}n!}\frac{\bar{\gamma}_2^{\alpha(v-\mu)/2}}{\mu^v}\gamma\left(v,\mu\left(\frac{x}{\bar{\gamma}_2}\right)^{\alpha/2}\right), & x\le\gamma_T \quad (18a)\\ \dfrac{\alpha\mu^\mu\left(\frac{x}{\bar{\gamma}_2}\right)^{\alpha\mu/2-1}\exp\left(-\mu\left(\frac{x}{\bar{\gamma}_2}\right)^{\alpha/2}\right)}{2\bar{\gamma}_2\Gamma(\mu)}-\dfrac{\mu^\mu m^m}{\Gamma(\mu)\Gamma(m)}\displaystyle\sum_{j=0}^{\infty}\sum_{k=0}^{\infty}\sum_{i=0}^{j+k+1}\binom{j+k+1}{i}\frac{K^j d_j}{(j!)^2}\times\frac{(-1)^{j+2k-i}i x^{i-1}}{k!(j+1+k)(2\sigma^2)^{j+k+1}}\frac{\bar{\gamma}_2^{\alpha(w-\mu)/2}}{\mu^w}\gamma\left(w,\mu\left(\frac{\gamma_T}{\bar{\gamma}_2}\right)^{\alpha/2}\right), & x>\gamma_T \quad (18b)\end{cases}$$

$$F_{\gamma_{\text{eff}}}(x)=\begin{cases}\dfrac{\mu^\mu m^m}{\Gamma(\mu)\Gamma(m)}\displaystyle\sum_{j=0}^{\infty}\sum_{n=0}^{\infty}\sum_{k=0}^{\infty}\sum_{i=0}^{j}\binom{j}{i}\frac{K^j d_j}{(j!)^2 n!k!}(-1)^{i+k}\times\frac{\mu^k}{(v+k)\bar{\gamma}_2^{\alpha(k+\mu)/2}}\frac{\gamma(\alpha(v+k)/2+j-i+1,\frac{x}{2\sigma^2})}{(2\sigma^2)^{n-\alpha(v+k)/2+i}}, & x\le\gamma_T \quad (24a)\\ \dfrac{\Gamma\left(\mu,\mu\left(\frac{\gamma_T}{\bar{\gamma}_2}\right)^{\alpha/2}\right)}{\Gamma(\mu)}-\dfrac{\Gamma\left(\mu,\mu\left(\frac{x}{\bar{\gamma}_2}\right)^{\alpha/2}\right)}{\Gamma(\mu)}-\dfrac{\mu^\mu m^m}{\Gamma(\mu)\Gamma(m)}\displaystyle\sum_{j=0}^{\infty}\sum_{k=0}^{\infty}\sum_{i=0}^{j+k+1}\binom{j+k+1}{i}\frac{K^j d_j}{(j!)^2}\times\frac{(-1)^{j+2k-i}x^i}{k!(j+1+k)(2\sigma^2)^{j+k+1}}\frac{\bar{\gamma}_2^{\alpha(w-\mu)/2}}{\mu^w}\gamma\left(w,\mu\left(\frac{\gamma_T}{\bar{\gamma}_2}\right)^{\alpha/2}\right), & x>\gamma_T \quad (24b)\end{cases}$$

The lower incomplete gamma function in (27) can be replaced with its series form as follows [37, eq. (3.381.2)]

$$\gamma\left(v,\mu\left(\frac{y}{\bar{\gamma}_2}\right)^{\alpha/2}\right)=\sum_{k=0}^{\infty}(-1)^k\frac{\mu^{v+k}}{k!(v+k)}\left(\frac{y}{\bar{\gamma}_2}\right)^{\alpha(v+k)/2} \tag{28}$$

Introducing (28) in (27) and simplifying yields

$$F_{\gamma_{\text{eff}}}(x)=\frac{\mu^\mu m^m}{\Gamma(\mu)\Gamma(m)}\sum_{j=0}^{\infty}\sum_{n=0}^{\infty}\sum_{k=0}^{\infty}\sum_{i=0}^{j}\binom{j}{i}\frac{K^j d_j}{(j!)^2 n!k!}\frac{(-1)^{i+k}}{(2\sigma^2)^{n+j+1}} \times\frac{\mu^k}{(v+k)\bar{\gamma}_2^{\alpha(k+\mu)/2}}\int_0^x y^{\alpha(v+k)/2+j-i}\exp\left(-\frac{y}{2\sigma^2}\right)dy,\ x\le\gamma_T \tag{29}$$

The integral in (29) can be solved with the aid of [37, eq. (3.381.1)] and thus (29) can be expressed as

$$F_{\gamma_{\text{eff}}}(x)=\frac{\mu^\mu m^m}{\Gamma(\mu)\Gamma(m)}\sum_{j=0}^{\infty}\sum_{n=0}^{\infty}\sum_{k=0}^{\infty}\sum_{i=0}^{j}\binom{j}{i}\frac{K^j d_j}{(j!)^2 n!k!}\frac{(-1)^{i+k}}{(2\sigma^2)^{n+j+1}} \times\frac{\mu^k}{(v+k)\bar{\gamma}_2^{\alpha(k+\mu)/2}}\frac{\gamma(\alpha(v+k)/2+j-i+1,\frac{x}{2\sigma^2})}{(2\sigma^2)^{-\alpha(v+k)/2-j+i-1}},\ x\le\gamma_T \tag{30}$$

Simplifying (30) yields (24a), which completes the proof for $\gamma_2\le\gamma_T$. When $\gamma_2>\gamma_T$ under MRC, the CDF of the output SNR γ_{eff} can be expressed as

$$F_{\gamma_{\text{eff}}}(x)=G(x)+F_{\gamma_2}(x)-F_{\gamma_2}(\gamma_T),\quad x>\gamma_T \tag{31}$$

where $G(x)$ can be calculated as [42, eqs. (6-38) and (6-42)]

$$G(x)=\int_0^{\gamma_T}\int_0^{x-z}f_{\gamma_1}(y)f_{\gamma_2}(z)dydz \tag{32}$$

$$=\int_0^{\gamma_T}f_{\gamma_2}(z)\left[\int_0^{x-z}f_{\gamma_1}(y)dy\right]dz \tag{33}$$

$$=\int_0^{\gamma_T}F_{\gamma_1}(x-z)f_{\gamma_2}(z)dz \tag{34}$$

$$=\frac{\alpha\mu^\mu m^m}{2\Gamma(\mu)\Gamma(m)\bar{\gamma}_2^{\alpha\mu/2}}\sum_{j=0}^{\infty}\frac{K^j d_j}{(j!)^2} \times\int_0^{\gamma_T}z^{\alpha\mu/2-1}\exp\left(-\mu\left(\frac{z}{\bar{\gamma}_2}\right)^{\alpha/2}\right)\gamma\left(j+1,\frac{x-z}{2\sigma^2}\right)dz \tag{35}$$

The lower incomplete gamma function in (35) can be replaced with its series form as follows [37, eq. (3.381.2)]

$$\gamma\left(j+1,\frac{x-z}{2\sigma^2}\right)=\sum_{k=0}^{\infty}(-1)^k\frac{1}{k!(j+k+1)}\left(\frac{x-z}{2\sigma^2}\right)^{j+k+1} \tag{36}$$

Using the binomial identity [37, eq. (1.111)] and simplifying, (36) can be written as

$$\gamma\left(j+1,\frac{x-z}{2\sigma^2}\right)=-\sum_{k=0}^{\infty}\sum_{i=0}^{j+k+1}\binom{j+k+1}{i}\frac{(-1)^{j+2k-i}x^i z^{j+k-i+1}}{k!(j+k+1)(2\sigma^2)^{j+k+1}} \tag{37}$$

Introducing (37) in (35) yields

$$G(x)=\frac{-\alpha\mu^\mu m^m}{2\Gamma(\mu)\Gamma(m)\bar{\gamma}_2^{\alpha\mu/2}}\sum_{j=0}^{\infty}\sum_{k=0}^{\infty}\sum_{i=0}^{j+k+1}\binom{j+k+1}{i}\frac{K^j d_j}{(j!)^2} \times\frac{(-1)^{j+2k-i}x^i}{k!(j+1+k)(2\sigma^2)^{j+k+1}}\int_0^{\gamma_T}z^{\alpha\mu/2+j+k-i}\exp\left(-\mu\left(\frac{z}{\bar{\gamma}_2}\right)^{\alpha/2}\right)dz \tag{38}$$

The integral in (38) can be solved with the aid of [37, eq. (3.381.8)], and simplifying the result yields

$$G(x)=\frac{-\mu^\mu m^m}{\Gamma(\mu)\Gamma(m)}\sum_{j=0}^{\infty}\sum_{k=0}^{\infty}\sum_{i=0}^{j+k+1}\binom{j+k+1}{i}\frac{K^j d_j}{(j!)^2} \times\frac{(-1)^{j+2k-i}x^i}{k!(j+1+k)(2\sigma^2)^{j+k+1}}\frac{\bar{\gamma}_2^{\alpha(w-\mu)/2}}{\mu^w}\gamma\left(w,\mu\left(\frac{\gamma_T}{\bar{\gamma}_2}\right)^{\alpha/2}\right) \tag{39}$$

where $w=\frac{\alpha\mu+2j+2k-2i+2}{\alpha}$.
Introducing (39) and (6) in (31) yields (24b), which completes the proof for $\gamma_2>\gamma_T$.

□

IV. PERFORMANCE ANALYSIS

A. PROBABILITIES OF OUTAGE AND LINK USAGE

The key performance parameters of URLLC are reliability and latency. Reliability is defined as the probability of a data packet being successfully transmitted within a certain time period while latency is the time taken for a data packet to be sent from the transmitter to the intended recipient. As highlighted in Section I, the primary focus of this study is on ensuring the reliability of URLLC systems. However, even if latency is not explicitly included, reducing the probability of outage can guarantee URLLC as discussed in [43]. Hence, the probability of outage is recognised as an effective metric for measuring the reliability of URLLC systems.

The probability of the proposed transmission system experiencing an outage is defined as the probability that the instantaneous effective SNR at the destination, γ_{eff}, falls below a specified outage threshold, γ_{out}, which represents the minimum SNR required to ensure the maximum allowable BER is not exceeded. This probability can be represented as $P_{\text{out}}=P(\gamma_{\text{eff}}\le\gamma_{\text{out}})=F_{\gamma_{\text{eff}}}(\gamma_{\text{out}})$, where $F_{\gamma_{\text{eff}}}(\cdot)$ is the CDF of the effective SNR at the destination as given by (9) and (24) for SC and MRC, respectively. In the proposed hybrid transmission scheme, the THz link is used for transmission with probability one. On the other hand, the mmWave link is used for transmission only when the quality of the THz link degrades (in terms of the instantaneous SNR γ_2). The probability of the mmWave link being used is expressed as $P_{\text{mmWave}}=P(\gamma_2\le\gamma_T)=F_{\gamma_2}(\gamma_T)$, where $F_{\gamma_2}(\cdot)$ is given by (6). A high P_{mmWave} means that the mmWave link needs to be used frequently as a backup for the THz link.

B. AVERAGE BIT ERROR RATE

For a given fading channel, the Average Bit Error Rate (ABER), $\overline{P}_b$, can be obtained as [44, eq. (8.102)]

$$\overline{P}_b = \int_0^\infty P_b(x) f_\gamma(x) dx, \tag{40}$$

where $P_b(\gamma)$ denotes the conditional bit-error probability for a given SNR γ and $f_\gamma(\cdot)$ represents the PDF of the instantaneous SNR per symbol. Binary modulations will be considered in this section, without loss of generality, using the following expression [45, eq. (13)]

$$P_b(\gamma) = \frac{\Gamma(b, a\gamma)}{2\Gamma(b)}, \tag{41}$$

where $\Gamma(\cdot,\cdot)$ represents the upper incomplete gamma function [37, eq. (8.350.2)] and $a, b \in \{\frac{1}{2}, 1\}$ are modulation-dependent parameters (see [44, Table 8.1] for more details). Based on (41), the ABER in (40) for binary modulations under a given fading channel can be expressed alternatively as [36, eq. (15)]

$$\overline{P}_b = \frac{a^b}{2\Gamma(b)} \int_0^\infty e^{-ax} x^{b-1} F_\gamma(x) dx \tag{42}$$

The solution to the integral in (42) for the backup link (based on the FTR model) is provided in [36, eq. (16)] together with [38, eq. (16)]. The solution to the integral in (42) for the main link (based on the $\alpha-\mu$ model) is provided below.

Theorem 5 (ABER for the $\alpha-\mu$ channel)**.** *The ABER of the $\alpha-\mu$ channel is given by (43).*

Proof. Introducing (6) in (42) yields

$$\overline{P}_b = \frac{a^b}{2\Gamma(b)} \int_0^\infty e^{-ax} x^{b-1} \left[1 - \frac{\Gamma\left(\mu, \mu\left(\frac{x}{\bar{\gamma}_2}\right)^{\alpha/2}\right)}{\Gamma(\mu)} \right] dx \tag{44}$$

By distributing the integral in (44) and with the aid of [37, eq. (3.381.4)], (44) can be expressed as

$$\overline{P}_b = \frac{a^b}{2\Gamma(b)} \left[\frac{\Gamma(b)}{a^b} - \frac{1}{\Gamma(\mu)} I \right] \tag{45}$$

where

$$I = \int_0^\infty e^{-ax} x^{b-1} \Gamma\left(\mu, \mu\left(\frac{x}{\bar{\gamma}_2}\right)^{\alpha/2}\right) dx \tag{46}$$

With the aid of [46, eqs. (8.4.3.1) and (8.4.16.2)], (46) can be written as follows

$$I = \int_0^\infty x^{b-1} G_{0,1}^{1,0}\left[ax \middle| \begin{matrix} - \\ 0 \end{matrix}\right] G_{1,2}^{2,0}\left[\frac{\mu}{\bar{\gamma}_2^{\alpha/2}} x^{\alpha/2} \middle| \begin{matrix} 1 \\ \mu, 0 \end{matrix}\right] dx \tag{47}$$

where $G_{p,q}^{m,n}\left(z \middle| \begin{matrix} a_r \\ b_s \end{matrix}\right)$ is the Meijer G-function given by [37, eq. (9.301)]. For even α, the solution to the integral in (47) can be obtained with the aid of [46, eq. (2.23.1-1)], which yields

$$I = \frac{(\alpha/2)^{\frac{1}{2}+b-1} a^{-b}}{(\sqrt{2\pi})^{\alpha/2-1}} G_{1+\alpha/2,2}^{2,\alpha/2}\left[\frac{\frac{\mu}{\bar{\gamma}_2^{\alpha/2}}}{a^{\alpha/2}(\alpha/2)^{-\alpha/2}} \middle| \begin{matrix} 1, \Delta(\alpha/2, 1-b) \\ \mu, 0 \end{matrix}\right] \tag{48}$$

where $\Delta(A,B) = \left\{\frac{B}{A}, \frac{B+1}{A}, ..., \frac{B+A-1}{A}\right\}$. Introducing (48) in (45) and simplifying yields (43a). Similarly, for odd α, the solution to the integral in (47) can be obtained with the aid of [46, eq. (2.23.1-1)], which yields

$$I = \frac{2^{\mu-\frac{1}{2}} \alpha^{\frac{1}{2}+b-1} a^{-b}}{(\sqrt{2\pi})^{\alpha}} G_{2+\alpha,4}^{4,\alpha}\left[\frac{\frac{\mu^2}{\bar{\gamma}_2^{\alpha}} 2^{-2}}{a^{\alpha}\alpha^{-\alpha}} \middle| \begin{matrix} \Delta(\alpha, 1-b), \Delta(2,1) \\ \Delta(2,\mu), \Delta(2,0) \end{matrix}\right] \tag{49}$$

Introducing (49) in (45) and simplifying yields (43b), which completes the proof. □

For the proposed hybrid transmission scheme, (42) is calculated as

$$\overline{P}_b = \frac{a^b}{2\Gamma(b)} \int_0^{\gamma_T} e^{-ax} x^{b-1} F_{\gamma_{\text{eff}}}(x) dx \tag{50}$$

$$+ \frac{a^b}{2\Gamma(b)} \int_{\gamma_T}^\infty e^{-ax} x^{b-1} F_{\gamma_{\text{eff}}}(x) dx \tag{51}$$

where the expression for $F_{\gamma_{\text{eff}}}(x)$ in each integral is related to the corresponding SNR interval. The ABER expressions of the proposed hybrid scheme under SC and MRC can be obtained using (50) and (51) as discussed below.

Theorem 6 (ABER under SC)**.** *The ABER of the proposed hybrid system under SC is given by*

$$\overline{P}_b = K_1 + K_2 \tag{52}$$

where K_1 and K_2 are given by (53) and (54) at the bottom of the next page, respectively, $\vartheta_{k,n} = \alpha(k+n)/2 + b$ and $\vartheta_{k,n,i} = \alpha(k+n)/2 + i + b$.

Proof. Introducing (9a) in (50) yields

$$K_1 = \frac{a^b}{2\Gamma(b)} \frac{m^m}{\Gamma(m)} \sum_{j=0}^\infty \frac{K^j d_j}{(j!)^2} \times \int_0^{\gamma_T} e^{-ax} x^{b-1} \left(1 - \frac{\Gamma\left(\mu, \mu\left(\frac{x}{\bar{\gamma}_2}\right)^{\alpha/2}\right)}{\Gamma(\mu)} \right) \gamma\left(j+1, \frac{x}{2\sigma^2}\right) dx \tag{55}$$

Distributing the integral in (55) and using the series forms for the incomplete gamma functions given by [37, eqs. (8.352.1) and (8.352.2)], (55) can be written as

$$\begin{aligned} K_1 =& \frac{a^b}{2\Gamma(b)}\frac{m^m}{\Gamma(m)}\sum_{j=0}^{\infty}\frac{K^j d_j}{j!} \\ &\times\left\{\int_0^{\gamma_T} e^{-ax}x^{b-1}\left[1-e^{-\frac{x}{2\sigma^2}}\sum_{i=0}^{j}\frac{x^i}{i!(2\sigma^2)^i}\right]dx\right. \\ &-\int_0^{\gamma_T} e^{-ax}x^{b-1}\left[e^{-\mu\left(\frac{x}{\bar{\gamma}_2}\right)^{\alpha/2}}\sum_{k=0}^{\mu-1}\frac{\mu^k}{k!}\left(\frac{x}{\bar{\gamma}_2}\right)^{\alpha k/2}\right] \\ &\left.\times\left[1-e^{-\frac{x}{2\sigma^2}}\sum_{i=0}^{j}\frac{x^i}{i!(2\sigma^2)^i}\right]dx\right\} \end{aligned} \tag{56}$$

$$\overline{P}_b = \begin{cases} \frac{1}{2}-\frac{1}{2\Gamma(b)\Gamma(\mu)}\frac{(\alpha/2)^{b-\frac{1}{2}}}{(\sqrt{2\pi})^{\alpha/2-1}}G^{2,\alpha/2}_{1+\alpha/2,2}\left[\frac{\mu(\alpha/2)^{\alpha/2}}{(a\bar{\gamma}_2)^{\alpha/2}}\middle|\begin{matrix}1,\Delta(\alpha/2,1-b)\\ \mu,0\end{matrix}\right], & \text{even } \alpha \quad (43a) \\ \frac{1}{2}-\frac{1}{2\Gamma(b)\Gamma(\mu)}\frac{2^{\mu-\frac{1}{2}}\alpha^{b-\frac{1}{2}}}{(\sqrt{2\pi})^{\alpha}}G^{4,\alpha}_{2+\alpha,4}\left[\frac{\mu^2\alpha^{\alpha}}{4(a\bar{\gamma}_2)^{\alpha}}\middle|\begin{matrix}\Delta(\alpha,1-b),\frac{1}{2},1\\ \frac{\mu}{2},\frac{\mu+1}{2},0,\frac{1}{2}\end{matrix}\right], & \text{odd } \alpha \quad (43b) \end{cases}$$

$$\begin{aligned} K_1 =& \frac{a^b}{2\Gamma(b)}\frac{m^m}{\Gamma(m)}\sum_{j=0}^{\infty}\frac{K^j d_j}{j!}\times\left\{\left[a^{-b}\gamma(b,a\gamma_T)-\sum_{i=0}^{j}\frac{(a+\frac{1}{2\sigma^2})^{-(b+i)}\gamma(b+i,(a+\frac{1}{2\sigma^2})\gamma_T)}{i!(2\sigma^2)^i}\right]-\right. \\ &\left.\left[\sum_{k=0}^{\mu-1}\sum_{n=0}^{\infty}(-1)^n\frac{\mu^{k+n}}{k!n!\bar{\gamma}_2^{\alpha(k+n)/2}}a^{-\vartheta_{k,n}}\gamma(\vartheta_{k,n},a\gamma_T)-\sum_{k=0}^{\mu-1}\sum_{i=0}^{j}\sum_{n=0}^{\infty}(-1)^n\frac{\mu^{k+n}}{\bar{\gamma}_2^{\alpha(k+n)/2}}\frac{(a+\frac{1}{2\sigma^2})^{-\vartheta_{k,n,i}}}{k!n!i!(2\sigma^2)^i}\gamma(\vartheta_{k,n,i},(a+\frac{1}{2\sigma^2})\gamma_T)\right]\right\} \end{aligned} \tag{53}$$

$$\begin{aligned} K_2 =& -\frac{a^b}{2\Gamma(b)}\sum_{k=0}^{\mu-1}\sum_{n=0}^{\infty}\frac{(-1)^n}{k!n!}\frac{\mu^{k+n}}{\bar{\gamma}_2^{\alpha(k+n)/2}}a^{-\vartheta_{k,n}}\Gamma(\vartheta_{k,n},a\gamma_T)+\frac{a^b m^m}{2\Gamma(b)\Gamma(m)}\left(1-\frac{\Gamma\left(\mu,\mu\left(\frac{\gamma_T}{\bar{\gamma}_2}\right)^{\alpha/2}\right)}{\Gamma(\mu)}\right)\times \\ &\sum_{j=0}^{\infty}\frac{K^j d_j}{j!}\left[a^{-b}\Gamma(b,a\gamma_T)-\sum_{i=0}^{j}\frac{1}{i!(2\sigma^2)^i}(a+\frac{1}{2\sigma^2})^{-(i+b)}\Gamma(i+b,(a+\frac{1}{2\sigma^2})\gamma_T)\right]+\frac{\Gamma(b,a\gamma_T)}{2\Gamma(b)\Gamma(\mu)}\Gamma\left(\mu,\mu\left(\frac{\gamma_T}{\bar{\gamma}_2}\right)^{\alpha/2}\right) \end{aligned} \tag{54}$$

$$T_1 = \frac{\mu^{\mu}m^m}{2\Gamma(b)\Gamma(\mu)\Gamma(m)}\sum_{j=0}^{\infty}\sum_{n=0}^{\infty}\sum_{k=0}^{\infty}\sum_{\ell=0}^{\infty}\sum_{i=0}^{j}\binom{j}{i}\frac{K^j d_j}{(j!)^2 n!k!\ell!}(-1)^{i+k+\ell}\times\mu^k\frac{(2\sigma^2)^{\alpha(v+k)/2-n-i-s-\ell}}{(v+k)(s+\ell)\bar{\gamma}_2^{\alpha(k+\mu)/2}}a^{-(s+\ell)}\gamma(s+\ell+b,a\gamma_T) \tag{62}$$

$$\begin{aligned} T_2 =& \frac{\Gamma\left(\mu,\mu\left(\frac{\gamma_T}{\bar{\gamma}_2}\right)^{\alpha/2}\right)}{2\Gamma(b)\Gamma(\mu)}\Gamma(b,a\gamma_T)-\frac{1}{2\Gamma(b)}\sum_{\ell=0}^{\mu-1}\sum_{n=0}^{\infty}\frac{\mu^{n+\ell}}{n!\ell!}\frac{(-1)^n}{(a\bar{\gamma}_2)^{\alpha(n+\ell)/2}}\Gamma(\alpha(n+\ell)/2,a\gamma_T) \\ &-\frac{\mu^{\mu}m^m}{2\Gamma(b)\Gamma(\mu)\Gamma(m)}\sum_{j=0}^{\infty}\sum_{k=0}^{\infty}\sum_{i=0}^{j+k+1}\binom{j+k+1}{i}\frac{K^j d_j}{(j!)^2 k!}\times\frac{(-1)^{j+2k-i}}{(j+k+1)(2\sigma^2)^{j+k+1}}\frac{\bar{\gamma}_2^{\alpha(w-\mu)/2}}{\mu^w}\gamma\left(w,\mu\left(\frac{\gamma_T}{\bar{\gamma}_2}\right)^{\alpha/2}\right)a^{-i}\Gamma(b+i,a\gamma_T) \end{aligned} \tag{63}$$

Distributing the integrals in (56) and using the infinite series representation for the exponential function [37, eq. (1.211)], (56) can be rewritten as

$$\begin{aligned}K_1 =&\frac{a^b}{2\Gamma(b)}\frac{m^m}{\Gamma(m)}\sum_{j=0}^{\infty}\frac{K^j d_j}{j!}\\&\times\left\{\left[\int_0^{\gamma_T}x^{b-1}e^{-ax}dx-\sum_{i=0}^{j}\frac{1}{i!(2\sigma^2)^i}\int_0^{\gamma_T}x^{b+i-1}e^{-ax-\frac{x}{2\sigma^2}}dx\right]\right.\\&-\left[\sum_{k=0}^{\mu-1}\sum_{n=0}^{\infty}(-1)^n\frac{\mu^{k+n}}{k!n!\bar{\gamma}_2^{\alpha(k+n)/2}}\int_0^{\gamma_T}x^{\alpha(k+n)/2+b-1}e^{-ax}dx\right.\\&-\sum_{k=0}^{\mu-1}\sum_{i=0}^{j}\sum_{n=0}^{\infty}(-1)^n\frac{\mu^{k+n}}{\bar{\gamma}_2^{\alpha(k+n)/2}}\frac{1}{k!n!i!(2\sigma^2)^i}\\&\left.\left.\times\int_0^{\gamma_T}x^{\alpha(k+n)/2+i+b-1}e^{-(\frac{1}{2\sigma^2}+a)x}dx\right]\right\}\end{aligned}\tag{57}$$

With the aid of [37, eq. (3.381.1)], K_1 can be obtained as given by (53). Similarly, K_2 can be obtained by introducing (9b) in (51) as follows

$$\begin{aligned}K_2 =&\frac{a^b}{2\Gamma(b)}\int_{\gamma_T}^{\infty}e^{-ax}x^{b-1}\left(1-\frac{\Gamma\left(\mu,\mu\left(\frac{x}{\bar{\gamma}_2}\right)^{\alpha/2}\right)}{\Gamma(\mu)}\right)dx\\&+\frac{a^b}{2\Gamma(b)}\left(1-\frac{\Gamma\left(\mu,\mu\left(\frac{\gamma_T}{\bar{\gamma}_2}\right)^{\alpha/2}\right)}{\Gamma(\mu)}\right)\\&\times\int_{\gamma_T}^{\infty}e^{-ax}x^{b-1}\left(\frac{m^m}{\Gamma(m)}\sum_{j=0}^{\infty}\frac{K^j d_j}{(j!)^2}\gamma\left(j+1,\frac{x}{2\sigma^2}\right)-1\right)dx\end{aligned}\tag{58}$$

Rearranging (58) and using the series forms for the incomplete gamma functions given by [37, eqs. (8.352) and (8.352.2)], (58) can be written as

$$\begin{aligned}K_2 =&\tfrac{a^b}{2\Gamma(b)}\int_{\gamma_T}^{\infty}e^{-ax}x^{b-1}dx-\tfrac{a^b}{2\Gamma(b)}\int_{\gamma_T}^{\infty}e^{-ax}x^{b-1}e^{-\mu\left(\frac{x}{\bar{\gamma}_2}\right)^{\alpha/2}}\sum_{k=0}^{\mu-1}\tfrac{\mu^k}{k!}\left(\tfrac{x}{\bar{\gamma}_2}\right)^{\alpha k/2}dx\\&+\frac{a^b}{2\Gamma(b)}\left(1-\frac{\Gamma\left(\mu,\mu\left(\frac{\gamma_T}{\bar{\gamma}_2}\right)^{\alpha/2}\right)}{\Gamma(\mu)}\right)\\&\times\left[\frac{m^m}{\Gamma(m)}\sum_{j=0}^{\infty}\frac{K^j d_j}{(j!)^2}\int_{\gamma_T}^{\infty}e^{-ax}x^{b-1}j!\left[1-e^{-\frac{x}{2\sigma^2}}\sum_{i=0}^{j}\frac{x^i}{i!(2\sigma^2)^i}\right]dx\right.\\&\left.-\int_{\gamma_T}^{\infty}e^{-ax}x^{b-1}dx\right]\end{aligned}\tag{59}$$

Using the infinite series representation for the exponential function [37, eq. (1.211)], (59) can be written as

$$\begin{aligned}K_2 =&-\frac{a^b}{2\Gamma(b)}\sum_{k=0}^{\mu-1}\sum_{n=0}^{\infty}(-1)^n\frac{\mu^n}{\bar{\gamma}_2^{n\alpha/2}}\frac{\mu^k}{k!n!\bar{\gamma}_2^{\alpha k/2}}\int_{\gamma_T}^{\infty}x^{\alpha(k+n)/2+b-1}e^{-ax}dx\\&+\frac{a^b m^m}{2\Gamma(b)\Gamma(m)}\left(1-\frac{\Gamma\left(\mu,\mu\left(\frac{\gamma_T}{\bar{\gamma}_2}\right)^{\alpha/2}\right)}{\Gamma(\mu)}\right)\sum_{j=0}^{\infty}\frac{K^j d_j}{j!}\left[\int_{\gamma_T}^{\infty}e^{-ax}x^{b-1}dx\right.\\&\left.-\sum_{i=0}^{j}\frac{1}{i!(2\sigma^2)^i}\int_{\gamma_T}^{\infty}e^{-ax-\frac{x}{2\sigma^2}}x^{i+b-1}dx\right]\\&+\frac{a^b}{2\Gamma(b)\Gamma(\mu)}\Gamma\left(\mu,\mu\left(\frac{\gamma_T}{\bar{\gamma}_2}\right)^{\alpha/2}\right)\int_{\gamma_T}^{\infty}e^{-ax}x^{b-1}dx\end{aligned}\tag{60}$$

With the aid of [37, eq. (3.381.3)], K_2 can be obtained as given by (54), which completes the proof. □

Theorem 7 (ABER under MRC)**.** *The ABER of the proposed hybrid system under MRC is given by*

$$\overline{P}_b = T_1 + T_2 \tag{61}$$

where T_1 and T_2 are given by (62) and (63) at the bottom of the previous page, respectively, and $s=\alpha(v+k)/2+j-i+1$.

Proof. Introducing (24a) in (50) yields

$$\begin{aligned}T_1 =&\frac{a^b}{2\Gamma(b)}\frac{\mu^\mu m^m}{\Gamma(\mu)\Gamma(m)}\sum_{j=0}^{\infty}\sum_{n=0}^{\infty}\sum_{k=0}^{\infty}\sum_{i=0}^{j}\binom{j}{i}\frac{K^j d_j}{(j!)^2 n!k!}(-1)^{i+k}\\&\times\frac{\mu^k}{(v+k)\bar{\gamma}_2^{\alpha(k+\mu)/2}}\int_0^{\gamma_T}e^{-ax}x^{b-1}\frac{\gamma(\alpha(v+k)/2+j-i+1,\frac{x}{2\sigma^2})}{(2\sigma^2)^{n-\alpha(v+k)/2+i}}dx\end{aligned}\tag{64}$$

Replacing the lower incomplete gamma function in (64) with its series form [37, eq. (3.381.2)] and rearranging, (64) can be expressed as

$$\begin{aligned}T_1 =&\frac{a^b}{2\Gamma(b)}\frac{\mu^\mu m^m}{\Gamma(\mu)\Gamma(m)}\sum_{j=0}^{\infty}\sum_{n=0}^{\infty}\sum_{k=0}^{\infty}\sum_{\ell=0}^{\infty}\sum_{i=0}^{j}\binom{j}{i}\frac{K^j d_j}{(j!)^2 n!k!\ell!}(-1)^{i+k+\ell}\\&\times\mu^k\frac{(2\sigma^2)^{\alpha(v+k)/2-n-i-s-\ell}}{(v+k)(s+\ell)\bar{\gamma}_2^{\alpha(k+\mu)/2}}\int_0^{\gamma_T}e^{-ax}x^{s+\ell+b-1}dx\end{aligned}\tag{65}$$

where $s=\alpha(v+k)/2+j-i+1$.
With the aid of [37, eq. (3.381.1)] and simplifying, T_1 can be obtained as given by (62). Similarly, T_2 can be obtained by introducing (24b) in (51) as follows

$$\begin{aligned}T_2 =&\frac{a^b}{2\Gamma(b)}\int_{\gamma_T}^{\infty}e^{-ax}x^{b-1}\left\{\frac{\Gamma\left(\mu,\mu\left(\frac{\gamma_T}{\bar{\gamma}_2}\right)^{\alpha/2}\right)}{\Gamma(\mu)}-\frac{\Gamma\left(\mu,\mu\left(\frac{x}{\bar{\gamma}_2}\right)^{\alpha/2}\right)}{\Gamma(\mu)}\right.\\&-\frac{\mu^\mu m^m}{\Gamma(\mu)\Gamma(m)}\sum_{j=0}^{\infty}\sum_{k=0}^{\infty}\sum_{i=0}^{j+k+1}\binom{j+k+1}{i}\frac{K^j d_j}{(j!)^2}\\&\left.\times\frac{(-1)^{j+2k-i}x^i}{k!(j+1+k)(2\sigma^2)^{j+k+1}}\frac{\bar{\gamma}_2^{\alpha(w-\mu)/2}}{\mu^w}\gamma\left(w,\mu\left(\frac{\gamma_T}{\bar{\gamma}_2}\right)^{\alpha/2}\right)\right\}\end{aligned}\tag{66}$$

Distributing the integral in (66) and using the infinite series form of the upper incomplete gamma function [37, eq. (3.352.2)], (66) can be expressed as

$$T_2 = \frac{a^b}{2\Gamma(b)}\left\{\frac{\Gamma\left(\mu,\mu\left(\frac{\gamma_T}{\bar{\gamma}_2}\right)^{\alpha/2}\right)}{\Gamma(\mu)}\int_{\gamma_T}^{\infty} e^{-ax}x^{b-1}dx - \sum_{\ell=0}^{\mu-1}\frac{\mu^\ell}{\ell!\bar{\gamma}_2^{\alpha\ell/2}}\int_{\gamma_T}^{\infty} e^{-ax-\mu\left(\frac{x}{\bar{\gamma}_2}\right)^{\alpha/2}}x^{\alpha\ell+b-1}dx - \frac{\mu^\mu m^m}{\Gamma(\mu)\Gamma(m)}\sum_{j=0}^{\infty}\sum_{k=0}^{\infty}\sum_{i=0}^{j+k+1}\binom{j+k+1}{i}\frac{K^j d_j}{(j!)^2} \times \frac{(-1)^{j+2k-i}}{k!(j+1+k)(2\sigma^2)^{j+k+1}}\frac{\bar{\gamma}_2^{\alpha(w-\mu)/2}}{\mu^w}\gamma\left(w,\mu\left(\frac{\gamma_T}{\bar{\gamma}_2}\right)^{\alpha/2}\right)\int_{\gamma_T}^{\infty} e^{-ax}x^{b+i-1}dx\right\} \tag{67}$$

Using the infinite series representation for the exponential function [37, eq. (1.211)] and with the aid of [37, eq. (3.381.3)], (67) can be expressed as

$$T_2 = \frac{a^b}{2\Gamma(b)}\left\{\frac{\Gamma\left(\mu,\mu\left(\frac{\gamma_T}{\bar{\gamma}_2}\right)^{\alpha/2}\right)}{\Gamma(\mu)}a^{-b}\Gamma(b,a\gamma_T) - \sum_{\ell=0}^{\mu-1}\sum_{n=0}^{\infty}\frac{\mu^{n+\ell}}{n!\ell!}\frac{(-1)^n}{\bar{\gamma}_2^{\alpha(n+\ell)/2}}a^{-(\alpha(n+\ell)/2+b)} \times \Gamma(\alpha(n+\ell)/2+b,a\gamma_T) - \frac{\mu^\mu m^m}{\Gamma(\mu)\Gamma(m)}\sum_{j=0}^{\infty}\sum_{k=0}^{\infty}\sum_{i=0}^{j+k+1}\binom{j+k+1}{i}\frac{K^j d_j}{(j!)^2} \times \frac{(-1)^{j+2k-i}}{k!(j+1+k)(2\sigma^2)^{j+k+1}}\frac{\bar{\gamma}_2^{\alpha(w-\mu)/2}}{\mu^w}\gamma\left(w,\mu\left(\frac{\gamma_T}{\bar{\gamma}_2}\right)^{\alpha/2}\right)a^{-(b+i)}\Gamma(b+i,a\gamma_T)\right\} \tag{68}$$

Expanding and simplifying terms, T_2 can be obtained as given by (63), which completes the proof. □

V. RESULTS

A. EVALUATION SCENARIO

Table 2 summarises the main evaluation parameters considered in this work. The FTR model is assumed for the backup link in the mmWave band, having a central frequency $f_1 = 28$ GHz [47, Table 5.2-1], while the $\alpha-\mu$ model is assumed for the main link in the THz band, having a central frequency $f_2 = 142$ GHz [40]. It is worth mentioning that the average SNR values in both links are not independent having the same physical propagation distance. In particular, the lower path loss associated to lower propagation frequencies leads to a higher average SNR in the mmWave link compared with the THz link. For both bands, the received power is calculated as $P_R = P_T\, G_T\, G_R\, [c/(4\pi f)]^2\, d^{-\delta}$, where P_T is the transmitted power, G_T and G_R are the gains of the transmitter and receiver antennas, respectively, $c = 3\times10^8$ m/s is the speed of light, f is the central frequency of each band (f_1 or f_2), d represents the physical separation between the transmitter and receiver antennas ($d = 100$ m by default unless otherwise stated), and $\delta = 3.4$ is the path loss exponent (under non-line-of-sight conditions for the mmWave and THz bands [34], [48]–[50]). The average SNR of each link ($\overline{\gamma}_1$ or $\overline{\gamma}_2$) is obtained as $\overline{\gamma} = P_R/P_N$, with the receiver's noise power calculated as $P_N = k_B T_0 B F$, where $k_B = 1.38\times10^{-23}$ J · K^{-1} is the Boltzmann constant, T_0 is the reference room temperature, B represents the bandwidth allocated to the link in each frequency band (B_1 or B_2) and F denotes the noise factor at the receiver (equivalent to a noise figure of 4 dB). The User Equipment (UE) channel bandwidth is assumed to be $B_1 = 50$ MHz for the mmWave link [47, Table 5.3.5-1] and $B_2 = 1$ GHz for the THz link [40].

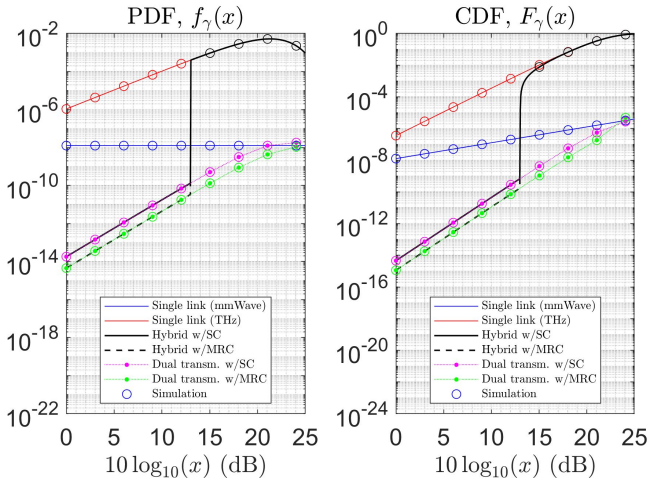

FIGURE 2. Validation of the SNR statistics ($d = 1000$ m).

TABLE 2. Evaluation parameters.

Parameter	Value
FTR model	$m = 20, K = 5, \Delta = 0.1$
$\alpha-\mu$ model	$\alpha = 3, \mu = 2$
Central frequency of the mmWave link (f_1)	28 GHz
Central frequency of the THz link (f_2)	142 GHz
Transmitted power (P_T)	40 dBm
Transmitter antenna gain (G_T)	40 dBi
Receiver antenna gain (G_R)	40 dBi
Path loss exponent (δ)	3.4
Reference room temperature (T_0)	290 K
UE channel bandwidth in the mmWave band (B_1)	50 MHz
UE channel bandwidth in the THz band (B_2)	1 GHz
Noise figure ($10\log_{10} F$)	4 dB

The general BER model of (41) is evaluated for $a = b = 1$ representing a differentially-encoded coherent BPSK modulation [44, Table 8.1]. Furthermore, the switching threshold of the proposed hybrid scheme is determined based on the condition that the maximum acceptable BER for accurate signal demodulation is 10^{-9}.

B. VALIDATION OF THE SNR STATISTICS

The accuracy of the mathematical analysis is validated by comparing the derived analytical expressions with Monte Carlo simulations ensuring consistency between theoretical and simulated results. This cross-validation confirms the reliability of the proposed model in characterising the hybrid THz/mmWave transmission scheme. In particular, the analytic results obtained in Section III are compared with their Monte Carlo simulation counterparts in Fig. 2. It is worth mentioning that logarithmic axes are used for improved level of detail in the low SNR regime. The proposed scheme defines the switching threshold as $\gamma_T = \gamma_{\text{out}}$, with γ_{out} being derived from (41). For a target BER of 10^{-9} and $a = b = 1$ the obtained switching threshold is $\gamma_T = 13$ dB. In Fig. 2, it can be seen that the effective SNR follows the PDF for the THz link for SNR values above γ_T. On the other hand, for

SNR values below γ_T, the effective SNR follows the PDF for the dual transmission scheme for both considered diversity techniques. Moreover, the analytic and simulation results are perfectly matched for all considered cases validating the correctness of the results provided in Section III.

Monte Carlo simulations will be employed to validate the outage probabilities and link usage results, whereas numerical integration will be used to validate the ABER results.

C. PERFORMANCE EVALUATION

Based on the outcomes of the analysis in Section IV, the performance of the proposed hybrid scheme is investigated and compared with suitable baseline scenarios. In particular, the performance is compared with the single link transmission and dual link transmission scenarios. The single link transmission implies the transmission over the THz link only and $\gamma_T = 0$ in this scenario. On the other hand, as $\gamma_T \to \infty$, the system transmits continuously over both links, namely as dual link transmission. For comparison reasons, the performance of transmitting over the mmWave link alone is provided as well.

The probability of outage versus the maximum tolerable BER is depicted in Fig. 3. It can be noticed that the probability of outage decreases as the tolerable BER increases. Transmitting over the THz link alone has the worst outage performance due to the high path loss associated with high propagation frequencies leading to a low average SNR. In addition, P_{out} decreases by transmitting over the mmWave link alone. However, it can be noticed that the most reliable transmission approach is achieved by transmitting continuously over the THz and mmWave links (dual transmission), which attains the best outage performance (as expected, MRC provides better outage performance than SC). The best outage performance can also be achieved by using the proposed hybrid scheme provided that the switching threshold condition $\gamma_T \geq \gamma_{\text{out}}$ is met. This condition ensures that the backup link is activated before the main link enters a state of outage. If this condition is not satisfied (i.e., $\gamma_T < \gamma_{\text{out}}$), then the system may temporarily fall in outage before the backup link is finally activated; in such case, the lower the switching threshold γ_T, the higher the outage probability, and therefore a more serious degradation is experienced in the reliability performance for lower values of γ_T. It is worth noting that a suitable selection for the switching threshold γ_T, meeting the condition $\gamma_T \geq \gamma_{\text{out}}$, plays a key role in the reliability performance as shown in Fig. 3. As long as such condition is satisfied, the proposed hybrid transmission scheme achieves the same level of reliability as the dual link transmission mode. Moreover, it is worth noting an extreme low level of outage probability is achieved under a few scenarios, meaning that the system is virtually free of outage. This can be explained as those numerical values are related to specific numerical configuration parameters and they could be higher or lower based on the considered operating conditions.

The probability of outage versus the distance between source and destination is depicted in Fig. 4. For a reliability

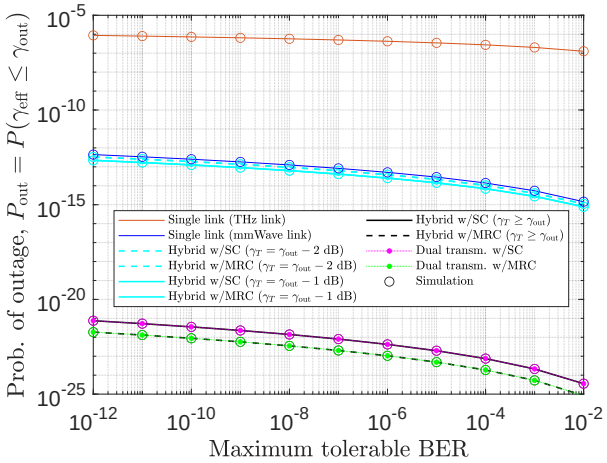

FIGURE 3. Outage probability versus maximum tolerable BER.

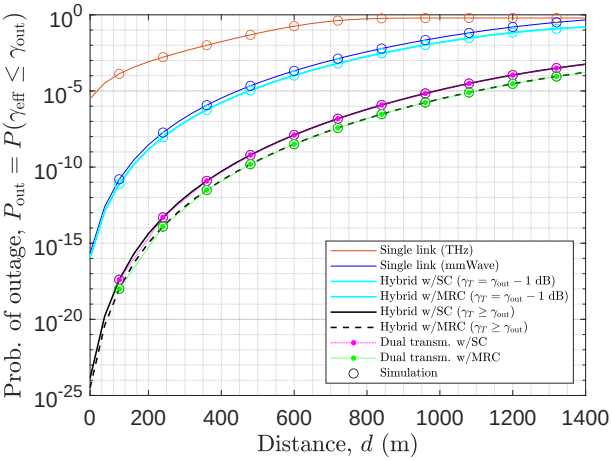

FIGURE 4. Outage probability versus communication distance.

requirement of $P_{\text{out}} = 10^{-5}$ (i.e., 99.999% link reliability), it can be noticed that a maximum communication distance of about 30 m can be achieved by transmitting over the main link (THz link) only. This communication distance can be increased by transmitting over both links (dual transmission) and by using the proposed hybrid transmission scheme to about 1000 m with SC diversity and 1100 m with MRC diversity. It is worth mentioning that the communication distances reported here are relatively long, but they are reasonable under specific operating conditions for such high frequencies [51], [52]. However, as shown in Fig. 5, the backup link (mmWave link) needs to be used, considering the proposed hybrid transmission scheme, around 1.2% and 3.1% of the time at 1000 m and 1100 m distances, respectively (for $\gamma_T = \gamma_{\text{out}} + 1$ dB). This means the backup link can be used for other data transmissions since it is available most of the time. Therefore, the proposed hybrid transmission scheme can increase the THz link communication range by 33/37-

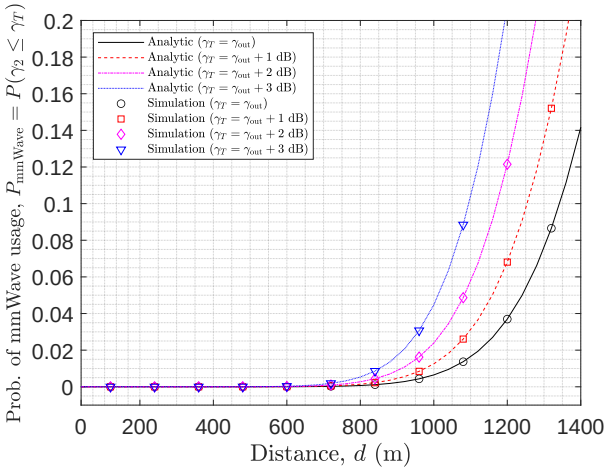

FIGURE 5. Backup link usage probability versus communication distance.

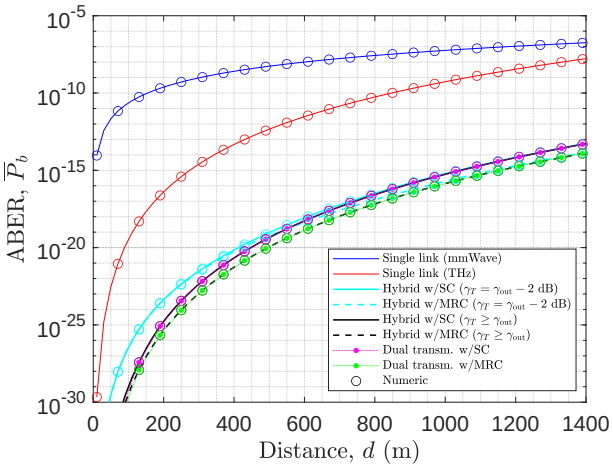

FIGURE 6. ABER versus communication distance.

fold by only reducing the availability of the mmWave link by 1.2%–3.1%. Consequently, the proposed hybrid transmission scheme achieves comparable link reliability to the dual transmission scheme while significantly improving resource efficiency.

It is interesting to mention that if the switching threshold γ_T increases above γ_{out}, the outage probability does not decrease further but the mmWave link usage increases (Fig. 5). Therefore, selecting the switching threshold as $\gamma_T = \gamma_{\text{out}}$ is considered the optimum choice in terms of the trade-off between system reliability and radio resource efficiency. However, due to hardware switching delays in practical systems, this optimum value might possibly result in temporary outages degrading the outage performance as shown in Fig. 4 when $\gamma_T < \gamma_{\text{out}}$. As a result, a certain amount of safety margin such as $\gamma_T = \gamma_{\text{out}} + 1$ dB should be permitted to guarantee that the backup link is activated on time, which would lead to a slight expense in the backup usage availability.

The ABER versus the distance between source and destination is depicted in Fig. 6. It can be noticed that Figs. 4 and 6 have the same trend, hence the same remarks apply. However, a major difference can be noticed when $\gamma_T < \gamma_{\text{out}}$. In particular, the ABER is not degraded as harshly as the outage performance for such values of γ_T. The explanation behind this is that $\overline{P}_b$ is an average of probabilities while P_{out} is the probability that a particular event occurs. Therefore, a small decrease in the switching threshold γ_T below the outage threshold γ_{out} would lead to a noticeable increase of outages and a slight increase in the rate of bit errors at the destination. In any case, the results in terms of both outage probability (Fig. 4) and ABER (Fig. 6) confirm that the proposed hybrid transmission scheme can provide the same level of reliability as the dual-link transmission approach, however with a significantly higher level of efficiency in the usage of radio resources (Fig. 5), thus making of it a suitable candidate for the efficient provision of URLLC services in current 5G and future 6G mobile communication systems.

VI. CONCLUSIONS

A novel hybrid THz/mmWave transmission scheme has been proposed to enhance the reliability of wireless communications in THz bands. The obtained results have shown that the proposed scheme can effectively enhance the reliability and achieve the same performance provided by the dual-link transmission scheme where both links (THz and mmWave) are used for transmission continuously, however with a significantly lower usage of the mmWave link, thus enhancing the usage of the available spectral resources. In general, the obtained results suggest that the proposed hybrid scheme can support the efficient provision of URLLC services in current 5G and future 6G mobile communication systems.

VII. FUTURE WORK

While the proposed hybrid transmission scheme significantly enhances URLLC reliability and efficiency, several avenues for future research remain open. First, incorporating additional parameters and exploring various deployment scenarios to provide a more comprehensive evaluation of the hybrid system's performance. Second, integrating additional frequency bands, such as sub-THz, could further improve adaptability and robustness. Third, the incorporation of machine learning-based link selection mechanisms could enable real-time predictive optimisation improving response to fluctuating channel conditions. Finally, experimental validation through testbed implementations would provide practical insights into real-world performance and deployment feasibility. These directions will be crucial for advancing URLLC technology and ensuring seamless high-frequency communication in future wireless networks.

ACKNOWLEDGEMENT

The authors extend their appreciation to the Deanship of Research and Graduate Studies at King Khalid University for funding this work through Small group Research Project under grant number RGP1/251/45.

REFERENCES

[1] A. Salh, L. Audah, N. S. M. Shah, A. Alhammadi, Q. Abdullah, Y. H. Kim, S. A. Al-Gailani, S. A. Hamzah, B. A. F. Esmail, and A. A. Almohammedi, "A survey on deep learning for ultra-reliable and low-latency communications challenges on 6G wireless systems," *IEEE Access*, vol. 9, pp. 55 098–55 131, Mar. 2021.

[2] R. Ali, Y. B. Zikria, A. K. Bashir, S. Garg, and H. S. Kim, "URLLC for 5G and beyond: requirements, enabling incumbent technologies and network intelligence," *IEEE Access*, vol. 9, pp. 67 064–67 095, Apr. 2021.

[3] X. Wang, L. Kong, F. Kong, F. Qiu, M. Xia, S. Arnon, and G. Chen, "Millimeter wave communication: a comprehensive survey," *IEEE Commun. Surveys Tuts.*, vol. 20, no. 3, pp. 1616–1653, Third Quarter 2018.

[4] V. Begishev, E. Sopin, D. Moltchanov, R. Pirmagomedov, A. Samuylov, S. Andreev, Y. Koucheryavy, and K. Samouylov, "Performance analysis of multi-band microwave and millimeter-wave operation in 5G NR systems," *IEEE Trans. Wireless Commun.*, vol. 20, no. 6, pp. 3475–3490, Jun. 2021.

[5] G. Noh, J. Kim, S. Choi, N. Lee, H. Chung, and I. Kim, "Feasibility validation of a 5G-enabled mmwave vehicular communication system on a highway," *IEEE Access*, vol. 9, pp. 36 535–36 546, Mar. 2021.

[6] M. A. Albreem, A. M. Sheikh, M. H. Alsharif, M. Jusoh, and M. N. M. Yasin, "Green Internet of Things (GIoT): applications, practices, awareness, and challenges," *IEEE Access*, vol. 9, pp. 38 833–38 858, Feb. 2021.

[7] T. H. L. Dinh, M. Kaneko, and K. Fujii, "Device selection and beamforming optimization in large-scale mmwave IoT networks," *IEEE Internet Things J.*, vol. 9, no. 24, pp. 25 395–25 408, Dec. 2022.

[8] B. Tezergil and E. Onur, "Wireless backhaul in 5G and beyond: issues, challenges and opportunities," *IEEE Commun. Surveys Tuts.*, vol. 24, no. 4, pp. 2579–2632, Fourth Quarter 2022.

[9] C. Chaccour, M. N. Soorki, W. Saad, M. Bennis, P. Popovski, and M. Debbah, "Seven defining features of terahertz (THz) wireless systems: a fellowship of communication and sensing," *IEEE Commun. Surveys Tuts.*, vol. 24, no. 2, pp. 967–993, Second Quarter 2022.

[10] T. S. Rappaport, Y. Xing, O. Kanhere, S. Ju, A. Madanayake, S. Mandal, A. Alkhateeb, and G. C. Trichopoulos, "Wireless communications and applications above 100 GHz: opportunities and challenges for 6G and beyond," *IEEE Access*, vol. 7, pp. 78 729–78 757, Jun. 2019.

[11] A. Shafie, N. Yang, C. Han, J. M. Jornet, M. Juntti, and T. Kürner, "Terahertz communications for 6G and beyond wireless networks: challenges, key advancements, and opportunities," *IEEE Netw.*, vol. 37, no. 3, pp. 162–169, Jun. 2023.

[12] A.-A. A. Boulogeorgos and A. Alexiou, "Error analysis of mixed THz-RF wireless systems," *IEEE Commun. Lett.*, vol. 24, no. 2, pp. 277–281, Feb. 2020.

[13] D. Moltchanov, E. Sopin, V. Begishev, A. Samuylov, Y. Koucheryavy, and K. Samouylov, "A tutorial on mathematical modeling of 5G/6G millimeter wave and terahertz cellular systems," *IEEE Commun. Surveys Tuts.*, vol. 24, no. 2, pp. 1072–1116, Second Quarter 2022.

[14] A.-A. A. Boulogeorgos, E. N. Papasotiriou, and A. Alexiou, "Analytical performance assessment of THz wireless systems," *IEEE Access*, vol. 7, pp. 11 436–11 453, Jan. 2019.

[15] A. S. Cacciapuoti, K. Sankhe, M. Caleffi, and K. R. Chowdhury, "Beyond 5G: THz-based medium access protocol for mobile heterogeneous networks," *IEEE Commun. Mag.*, vol. 56, no. 6, pp. 110–115, Jun. 2018.

[16] C.-X. Wang, J. Huang, H. Wang, X. Gao, X. You, and Y. Hao, "6G wireless channel measurements and models: trends and challenges," *IEEE Veh. Technol. Mag.*, vol. 15, no. 4, pp. 22–32, Dec. 2020.

[17] D. Serghiou, M. Khalily, T. W. C. Brown, and R. Tafazolli, "Terahertz channel propagation phenomena, measurement techniques and modeling for 6g wireless communication applications: a survey, open challenges and future research directions," *IEEE Commun. Surveys Tuts.*, vol. 24, no. 4, pp. 1957–1996, Fourth Quarter 2022.

[18] W. Jiang and H. D. Schotten, "Initial beamforming for millimeter-wave and terahertz communications in 6G mobile systems," in *Proc. IEEE Wireless Commun. Netw. Conf. (WCNC)*, Apr. 2022, pp. 2613–2618.

[19] C. She, Z. Chen, C. Yang, T. Q. S. Quek, Y. Li, and B. Vucetic, "Improving network availability of ultra-reliable and low-latency communications with multi-connectivity," *IEEE Trans. Commun.*, vol. 66, no. 11, pp. 5482–5496, Nov. 2018.

[20] G. S. Kesava and N. B. Mehta, "Multi-connectivity for URLLC and coexistence with eMBB in time-varying and frequency-selective fading channels," *IEEE Trans. Wireless Commun.*, vol. 22, no. 12, pp. 3599–3611, Jun. 2022.

[21] L. Chinchilla-Romero, J. Prados-Garzon, P. Muñoz, P. Ameigeiras, and J. M. Lopez-Soler, "URLLC achieved data rate through exploiting multi-connectivity in industrial private 5G networks with multi-WAT RANs," in *Proc. IEEE Wireless Commun. Netw. Conf. (WCNC)*, Mar. 2023, pp. 1–6.

[22] R. Liu, G. Yu, J. Yuan, and G. Y. Li, "Resource management for millimeter-wave ultra-reliable and low-latency communications," *IEEE Trans. Commun.*, vol. 69, no. 2, pp. 1094–1108, Feb. 2021.

[23] P. U. Adamu, M. López-Benítez, and J. Zhang, "Hybrid transmission scheme for improving link reliability in mmwave URLLC communications," *IEEE Trans. Wireless Commun.*, vol. 22, no. 9, pp. 6329–6340, Sep. 2023.

[24] M. Z. Chowdhury, M. K. Hasan, M. Shahjalal, M. T. Hossan, and Y. M. Jang, "Optical wireless hybrid networks: trends, opportunities, challenges, and research directions," *IEEE Commun. Surveys Tuts.*, vol. 22, no. 2, pp. 930–966, Second Quarter 2020.

[25] Z. Zhang, Q. Sun, M. López-Benítez, X. Chen, and J. Zhang, "Performance analysis of dual-hop RF/FSO relaying systems with imperfect CSI," *IEEE Trans. Veh. Technol.*, vol. 71, no. 5, pp. 4965–4976, May 2022.

[26] P. K. Singya, B. Makki, A. D'Errico, and M.-S. Alouini, "Hybrid FSO/THz-based backhaul network for mmwave terrestrial communication," *IEEE Trans. Wireless Commun.*, vol. 22, no. 7, pp. 4342–4359, Jul. 2023.

[27] T. Rakia, H.-C. Yang, M.-S. Alouini, and F. Gebali, "Outage analysis of practical FSO/RF hybrid system with adaptive combining," *IEEE Commun. Lett.*, vol. 19, no. 8, pp. 1366–1369, Jun. 2015.

[28] C. Wang and Y. J. Chun, "Stochastic geometric analysis of the terahertz (THz)-mmwave hybrid network with spatial dependence," *IEEE Access*, vol. 11, pp. 25 063–25 076, Jan. 2023.

[29] P. Bhardwaj and S. M. Zafaruddin, "Performance analysis of cooperative relaying for multi-antenna RF transmissions over THz wireless link," in *Proc. IEEE 95th Veh. Technol. Conf. (VTC-Spring)*, Jun. 2022, pp. 1–5.

[30] H. Du, J. Zhang, J. Cheng, and B. Ai, "Millimeter wave communications with reconfigurable intelligent surfaces: Performance analysis and optimization," *IEEE Trans. Commun.*, vol. 69, no. 4, pp. 2752–2768, Jan. 2021.

[31] N.-T. Nguyen, H.-N. Nguyen, N.-L. Nguyen, A.-T. Le, T. N. Nguyen, and M. Voznak, "Performance analysis of NOMA-based hybrid satellite-terrestrial relay system using mmWave technology," *IEEE Access*, vol. 11, pp. 10 696–10 707, Jan. 2023.

[32] C. Chaccour, R. Amer, B. Zhou, and W. Saad, "On the reliability of wireless virtual reality at terahertz (THz) frequencies," in *Proc. 10th IFIP Int. Conf. New Technol. Mobility and Secur. (NTMS)*, Jun. 2019, pp. 1–5.

[33] D. Ohmann, A. Awada, I. Viering, M. Simsek, and G. P. Fettweis, "Diversity trade-offs and joint coding schemes for highly reliable wireless transmissions," in *Proc. IEEE 84th Veh. Technol. Conf. (VTC-Fall)*, Sep. 2016, pp. 1–6.

[34] G. L. Stüber, *Principles of mobile communciation*, 4th ed. Springer, 2017.

[35] J. M. Romero-Jerez, F. J. Lopez-Martinez, J. F. Paris, and A. J. Goldsmith, "The fluctuating two-ray fading model: statistical characterization and performance analysis," *IEEE Trans. Wireless Commun.*, vol. 16, no. 7, pp. 4420–4432, Jul. 2017.

[36] J. Zhang, W. Zeng, X. Li, Q. Sun, and K. P. Peppas, "New results on the fluctuating two-ray model with arbitrary fading parameters and its applications," *IEEE Trans. Veh. Technol.*, vol. 67, no. 3, pp. 2766–2770, Mar. 2018.

[37] I. Gradshteyn and I. Ryzhik, *Table of integrals, series, and products*, 7th ed. London, UK: Academic Press, 2007.

[38] M. López-Benítez and J. Zhang, "Comments and corrections to new results on the fluctuating two-ray model with arbitrary fading parameters and its applications," *IEEE Trans. Veh. Technol.*, vol. 70, no. 2, pp. 1938–1940, Feb. 2021.

[39] M. D. Yacoub, "The α-μ distribution: A physical fading model for the stacy distribution," *IEEE Trans. Veh. Technol.*, vol. 56, no. 1, pp. 27–34, Jan. 2007.

[40] E. N. Papasotiriou, A.-A. A. Boulogeorgos, K. Haneda, M. F. de Guzman, and A. Alexiou, "An experimentally validated fading model for THz wireless systems," *Scientific Reports*, vol. 11, no. 1, p. 18717, 2021.

[41] A. M. Magableh and M. M. Matalgah, "Moment generating function of the generalized α-μ distribution with applications," *IEEE Commun. Lett.*, vol. 13, no. 6, pp. 411–413, Jun. 2009.

[42] A. Papoulis and S. U. Pillai, *Probability, random variables and stochastic processes*, 4th ed. McGraw Hill, 2001.

[43] P. Popovski, C. Stefanović, J. J. Nielsen, E. de Carvalho, M. Angjelichinoski, K. F. Trillingsgaard, and A.-S. Bana, "Wireless access in ultra-

reliable low-latency communication (URLLC)," *IEEE Trans. Commun.*, vol. 67, no. 8, pp. 5783–5801, Aug. 2019.
[44] M. K. Simon and M.-S. Alouini, *Digital communications over fading channels*, 2nd ed. Hoboken, NJ, USA: Wiley-IEEE Press, 2005.
[45] A. H. Wojnar, "Unknown bounds on performance in Nakagami channels," *IEEE Trans. Commun.*, vol. 34, no. 1, pp. 22–24, Jan. 1986.
[46] A. P. Prudnikov, I. U. A. Brychkov, and O. I. Marichev, *Integrals and Series: Special Functions, vol. 2*. London, UK: Gordon and Breach, 1986.
[47] 3rd Generation Partnership Project, "Technical Specification Group Radio Access Network; NR; User Equipment (UE) radio transmission and reception; Part 2: Range 2 Standalone (Release 17)," 3GPP, Tech. Rep. 3GPP TS 38.101-2, Mar. 2022, v17.5.0.
[48] A. I. Sulyman, A. T. Nassar, M. K. Samimi, G. R. MacCartney, T. S. Rappaport, and A. Alsanie, "Radio propagation path loss models for 5G cellular networks in the 28 GHz and 38 GHz millimeter-wave bands," *IEEE Commun. Mag.*, vol. 52, no. 9, pp. 78–86, Sep. 2014.
[49] M. K. Samimi, T. S. Rappaport, and G. R. MacCartney, "Probabilistic omnidirectional path loss models for millimeter-wave outdoor communications," *IEEE Wireless Commun. Lett.*, vol. 4, no. 4, pp. 357–360, Aug. 2015.
[50] S. Ju, Y. Xing, O. Kanhere, and T. S. Rappaport, "Sub-terahertz channel measurements and characterization in a factory building," in *Proc. IEEE Int. Conf. Commun. (ICC)*, May 2022, pp. 2882–2887.
[51] Y. Xing and T. S. Rappaport, "Millimeter wave and terahertz urban microcell propagation measurements and models," *IEEE Commun. Lett.*, vol. 25, no. 12, pp. 3755–3759, Dec. 2021.
[52] W. Li *et al.*, "Photonic terahertz wireless communication: Towards the goal of high-speed kilometer-level transmission," *J. Lightw. Technol.*, vol. 42, no. 3, pp. 1159–1172, Feb. 2024.

MOAWIAH ALHULAYIL (S'20, M'22) received the BSc and MSc degrees in Electrical Engineering from Jordan University of Science and Technology, Jordan in 2011 and 2014, respectively, and the PhD degree in Electrical Engineering and Electronics from University of Liverpool, UK in 2021. He became an Assistant Professor with the Department of Electrical Engineering, Applied Science Private University (ASU), Jordan since October 2021. From 2023 to 2024, he was the Head of Electrical Engineering Department, Faculty of Engineering & Technology, ASU, Jordan. From August 2022 to September 2022, he was a visiting researcher at the Department of Electrical Engineering and Electronics, University of Liverpool, UK. From June 2018 to July 2018, he was a visiting researcher at Centre Tecnològic de Telecomunicacions de Catalunya (CTTC), Barcelona, Spain. From 2017 to 2019, he was a Graduate Teaching Assistant in the Department of Electrical Engineering and Electronics, University of Liverpool, UK. His research interests include wireless cooperative networks, URLLC communications, cognitive radio, dynamic spectrum, and Cellular/Wi-Fi coexistence.

MOHAMMAD ABU AQOULAH received the BSc degree in Communication Engineering from Yarmouk University, Jordan in 2019, and the MSc degree in Electrical Engineering/Wireless Communications from Jordan University of Science and Technology, Jordan in 2023. During his master's studies, he also participated as an Erasmus+ Exchange Student at Friedrich Alexander University Erlangen-Nuremberg, Germany, in 2021. From 2021 to 2023, he was a Teaching Assistant in the Department of Electrical Engineering at Jordan University of Science and Technology, where he taught and supervised lab sessions and supported research projects. His research interests include 6G wireless communication, ultra-reliable low-latency communications (URLLC), and cognitive network technologies. Currently, he aims to advance innovations in wireless communication for 6G, focusing on enhancing efficiency, reliability, and security of next-generation networks.

MIGUEL LÓPEZ-BENÍTEZ (S'08, M'12, SM'17) received the BSc and MSc degrees (both with Distinction) in Telecommunication Engineering from Miguel Hernández University, Elche, Spain in 2003 and 2006, respectively, and the PhD degree (*summa cum laude*) in Telecommunication Engineering from the Technical University of Catalonia, Barcelona, Spain in 2011. From 2011 to 2013, he was a Research Fellow with the Centre for Communication Systems Research, University of Surrey, Guildford, UK. In 2013, he became a Lecturer (Assistant Professor) with the Department of Electrical Engineering and Electronics, University of Liverpool, UK, where he has been a Senior Lecturer (Associate Professor) since 2018. His research interests include the field of wireless communications and networking, with special emphasis on mobile communications and dynamic spectrum access in cognitive radio systems. He has been the Principal Investigator or Co-Investigator of research projects funded by the EPSRC, British Council, and Royal Society, and has also been involved in the European-funded projects AROMA, NEWCOM++, FARAMIR, QoSMOS, and CoRaSat. He has been a member of the Organising Committee for the IEEE WCNC International Workshop on Smart Spectrum since 2015 and is currently an Associate Editor of IEEE Access, IET Communications, and Wireless Communications and Mobile Computing. Personal website at http://www.lopezbenitez.es.

MAMOUN F. AL-MISTARIHI received his BSc and MSc degrees in Electrical Engineering from Jordan University of Science and Technology, Irbid, Jordan. M.E.E. and PhD degrees in Electrical Engineering from University of Minnesota, Minneapolis, MN, USA, in 1992, 1996, 2005, and 2005, respectively. From April 1994 to December 2000, he was with the Royal Scientific Society, Amman, Jordan. Presently he is a Professor with the Electrical Engineering Department, Jordan University of Science and Technology, Irbid, Jordan. His research interests include digital signal processing, image processing, digital signal processing for communications, wireless communication systems over fading channels, security of wireless systems, and wireless sensor networks.

MOHAMMED ALAMMAR (S'20, M'23) received the degrees of BSc in electrical engineering from the King Khalid University, KSA, in 2012, and MSc in electrical engineering from the University of Dayton, USA, in 2016. Additionally, the PhD degree in Electrical Engineering and Electronics from the University of Liverpool, UK, in 2023. He became a Lecturer (Assistant Professor) since October 2023 with the Department of Electrical Engineering, King Khalid University. From 2012 to 2018, he was a Graduate Teaching Assistant with the Department of Electrical Engineering, King Khalid University. From 2019 to 2022, he was a Senior Teaching Assistant (Assistant Lecturer) with the Department of Electrical Engineering, King Khalid University. His research interests include wireless communication and networking (with special emphasis on wireless sensor networks, cognitive radio and dynamic spectrum), Image Processing and Signal Processing.

ABDULRAHMAN AL AYIDH received his BSc degree in electrical engineering (Second honour) from King Khalid University, Abha, Saudi Arabia in 2014, and MSc (Distinction) in Telecommunication and Wireless Systems from University of Liverpool, UK in 2018. He obtained a PhD degree from the University of Glasgow, Glasgow, UK in 2022. His research interests include wireless communication systems, massive MIMO, cell free massive MIMO systems, hybrid beamforming techniques, ultra-reliable and low-latency communications, and wireless networked control system.